INFORMATION TO USERS

This dissertation was produced from a microfilm copy of the original document. While the most advanced technological means to photograph and reproduce this document have been used, the quality is heavily dependent upon the quality of the original submitted.

The following explanation of techniques is provided to help you understand markings or patterns which may appear on this reproduction.

1. The sign or "target" for pages apparently lacking from the document photographed is "Missing Page(s)". If it was possible to obtain the missing page(s) or section, they are spliced into the film along with adjacent pages. This may have necessitated cutting thru an image and duplicating adjacent pages to insure you complete continuity.

2. When an image on the film is obliterated with a large round black mark, it is an indication that the photographer suspected that the copy may have moved during exposure and thus cause a blurred image. You will find a good image of the page in the adjacent frame.

3. When a map, drawing or chart, etc., was part of the material being photographed the photographer followed a definite method in "sectioning" the material. It is customary to begin photoing at the upper left hand corner of a large sheet and to continue photoing from left to right in equal sections with a small overlap. If necessary, sectioning is continued again — beginning below the first row and continuing on until complete.

4. The majority of users indicate that the textual content is of greatest value, however, a somewhat higher quality reproduction could be made from "photographs" if essential to the understanding of the dissertation. Silver prints of "photographs" may be ordered at additional charge by writing the Order Department, giving the catalog number, title, author and specific pages you wish reproduced.

University Microfilms

300 North Zeeb Road
Ann Arbor, Michigan 48106

A Xerox Education Company

The electronic structure and Fermi surface of rhenium trioxide

by

Harold William Myron

A Dissertation Submitted to the
Graduate Faculty in Partial Fulfillment of
The Requirements for the Degree of
DOCTOR OF PHILOSOPHY

Department: Physics
Major: Solid State Physics

Approved:

Signature was redacted for privacy.

In Charge of Major Work

Signature was redacted for privacy.

For the Major Department

Signature was redacted for privacy.

For the Graduate College

Iowa State University
Ames, Iowa

1972

TABLE OF CONTENTS

INTRODUCTION

During the last ten years there has been much interest in the electrical and magnetic properties of the transition metal oxides. This class of compounds has members which are either insulators, metals or go through an insulator to metal transition with increasing temperature.

Rhenium trioxide was found to be an excellent metal by Ferretti et al. (1) having an electrical conductivity of $2.5 \times 10^6\ \Omega^{-1}\text{-cm}^{-1}$ at 77 K. At room temperature, the conductivity of ReO_3 approaches $10^5\ \Omega^{-1}\text{-cm}^{-1}$ which is within an order of magnitude of copper. Tungsten trioxide is an insulator having one less conduction electron per unit cell than ReO_3. However, when an extra conduction electron per unit cell is added to WO_3 by way of introducing a sodium atom the resulting compound $NaWO_3$ is metallic.

Tungsten's electronic configuration $5d^4 6s^2$ has one less 5d electron than rhenium. When sodium is added to WO_3, the primitive lattice becomes simple cubic with the sodium atoms located at the corners of the cube, and the WO_3 has the same structural configuration as ReO_3. The eight Na atoms, each having one 3s electron, are shared equally by eight nearest neighbor unit cells. This contributes one more conduction electron per unit cell. Thus ReO_3 and $NaWO_3$ have the same number of conduction electrons per unit cell.

Feinleib et al. (2) have reported that the optical spectrum of ReO_3 is quite similar to that of Na_xWO_3 $(.3 \lesssim x \lesssim 1.0)$. Thus a band picture which explains $NaWO_3$ should also be consistent with one that explains ReO_3. From Fromhold and Narath (3) and Feinleib et al. (2) the models

which attempt to explain the conduction bands of Na_xWO_3 are

1) Sienko (4) model: $5d(t_{2g})$ states from the tungsten;

2) Keller (5) model: 6s states from the tungsten;

3) Mackintosh (6) model: 3p states from the sodium;

4) Fuchs (7) model: 3p states from the sodium; and

5) Goodenough (8) model: π bonded oxygen and $5d(t_{2g})$ states from the tungsten.

Since there are no 3p states in the conduction band of ReO_3, models 3 and 4 can immediately be eliminated. Fromhold and Narath (3) and Narath and Barham (9) deduced from NMR studies on $NaWo_3$ and ReO_3 that the conduction band states at the Fermi level are not s-like but are derived mainly from atomic d states. Therefore, model 2 may also be excluded. In the present model we have included the s, p and d states of the rhenium atoms and the s, p and d states of the oxygen atoms. This seems to be consistent with models 1 and 5 and also with the experimental work.

Mattheiss (10,11) calculated the energy bands of ReO_3. His calculation was broken up into the following stages:

1) Calculating the energy levels at the high symmetry points of the Brillouin zone using nonrelativistic augmented plane wave method (APW);

2) Fitting the energy bands at the high symmetry points of the Brillouin zone by the Slater-Koster (12) interpolation scheme to determine the eigenvalues of the non-symmetry points;

3) Refitting the Slater-Koster parameters to correspond with the experimental data of Feinleib et al. (2) and Marcus (13).

In the present work we have also calculated the energy bands of

ReO_3 for the equilibrium lattice constant. Also, the equilibrium lattice constant given by Pearson (14) has been changed by 2% in order to determine the electronic properties of ReO_3 under pressure. This corresponds to a hydrostatic pressure of 113 kbar, from the bulk compressibility for ReO_3 determined by Schirber et al. (15). We have used the method developed by Segall (16) for calculating the energy bands of "complex crystals". A "complex crystal" has more than one atom per unit cell. Segall's method is a modification of the KKR method, developed independently by Korringa (17) and Kohn and Rostoker (18). Segall's method for calculating the matrix elements of a "complex crystal" is very slowly convergent. It became necessary to generalize a technique used by Ham and Segall (19), who derived a technique for faster convergence of the matrix elements for a crystal with one atom per unit cell. Using this method, the energy bands have been calculated for a uniform mesh in the Brillouin zone.

From the energy eigenvalues we were able to calculate the density of states and Fermi surface geometry of the ReO_3 crystal as a function of lattice parameter. The pressure derivatives of the de Haas-van Alphen frequencies have also been calculated and have been compared to experimental results (15). Finally, the de Haas-van Alphen frequencies have been calculated along the high symmetry directions.

THE STRUCTURE AND CRYSTAL POTENTIAL OF ReO_3

The Structure of Rhenium Trioxide

The rhenium trioxide unit cell is simple cubic as shown in Figure 1. The rhenium atom is located at the origin and the oxygen atoms are located at the face centers. There are four atoms per unit cell; the six oxygen atoms on the face centers are shared equally with their respective adjacent unit cells. The unit cell can then be thought of as a rhenium atom at the origin and three oxygen atoms on the cartesian coordinate axes as shown in Figure 2. The rhenium atom is located at the origin (0,0,0) and the oxygen atoms are at (a/2,0,0), (0,a/2,0), and (0,0,a/2), where a is the lattice constant.

The basic translation vectors of a simple cubic lattice are

$$\vec{r}_s = s_1\vec{a}_1 + s_2\vec{a}_2 + s_3\vec{a}_3 \tag{1}$$

where

$$\vec{a}_1 = a\hat{i},\ \vec{a}_2 = a\hat{j} \text{ and } \vec{a}_3 = a\hat{k} \tag{2}$$

and s_1, s_2, and s_3 are integers. The translation vectors are such that the crystal potential, which is periodic throughout the crystal, has the property that

$$V(\vec{r} + \vec{r}_s) = V(\vec{r}). \tag{3}$$

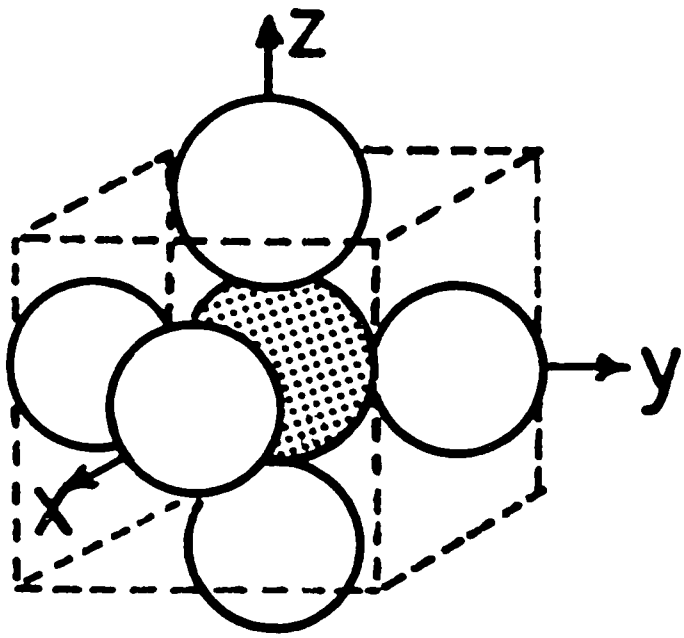

Figure 1. The unit cell of ReO_3. The white spheres are the oxygens and the dotted sphere is the rhenium.

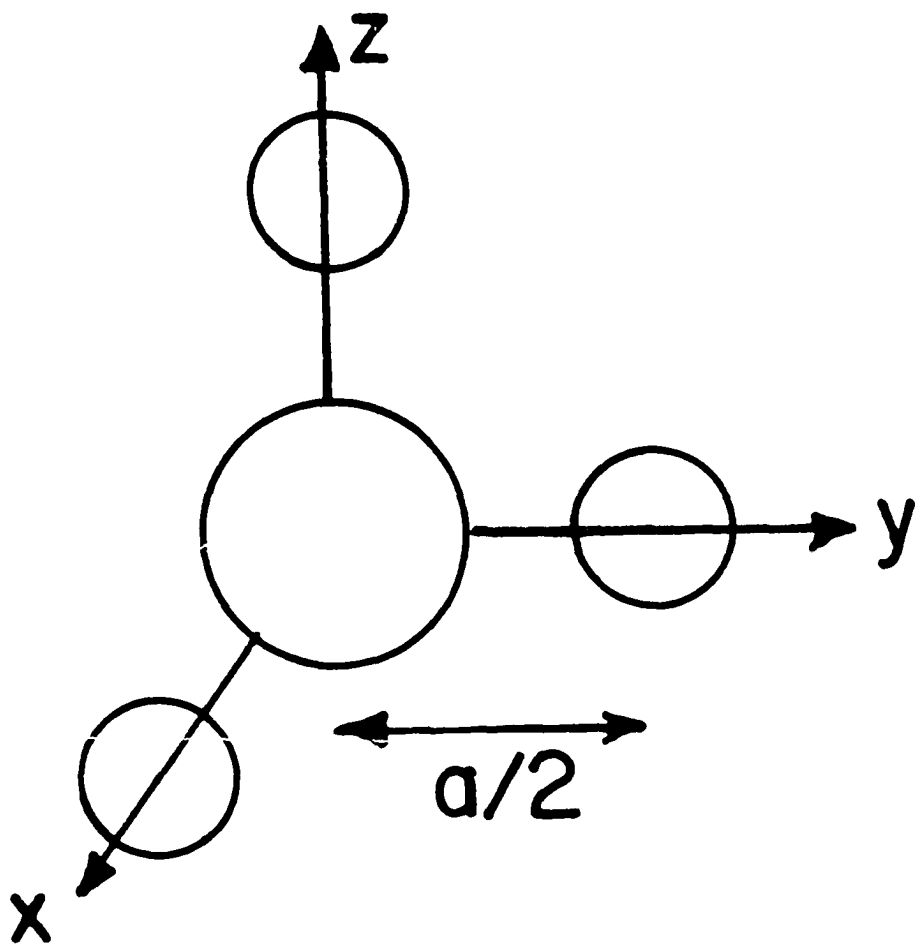

Figure 2. The rhenium atom is at the origin and the oxygen atoms are at (a/2,0,0)(0,a/2,0) and (0,0,a/2). The lattice parameter is a.

The reciprocal lattice vectors, the "recips", are defined as

$$\vec{K}_n = n_1\vec{A}_1 + n_2\vec{A}_2 + n_3\vec{A}_3 \tag{4}$$

where n_1, n_2 and n_3 are integers such that

$$\vec{K}_n \cdot \vec{r}_s = 2\pi\,[\text{integer}]. \tag{5}$$

This relationship is satisfied if $\vec{A}i \cdot \vec{a}j = 2\pi\delta_{ij}$. For a simple cubic lattice the Brillouin zone is also simple cubic as shown in Figure 3.

The Crystal Potential of Rhenium Trioxide

In order to calculate the electronic states of ReO_3 a crystal potential is constructed which is spherically symmetric within a radius, the muffin tin radius, and equal to a constant outside of this radius. This type of approximation to the crystal potential is called a muffin tin potential.

The muffin tin potential is calculated along the same lines first proposed by Mattheiss (20). Starting with the Hartree-Fock-Slater atomic charge densities calculated by Herman and Skillman (21) we solve Poisson's equation

$$\nabla^2 U_o^{\alpha}(|\vec{r} - \vec{r}_j|) = -8\pi\rho_{\alpha}(|\vec{r} - \vec{r}_j|) \tag{6}$$

where $\vec{r}_j$ is the position of the jth atom in the unit cell with respect to the origin. The potential due to one atom in the unit cell in atomic

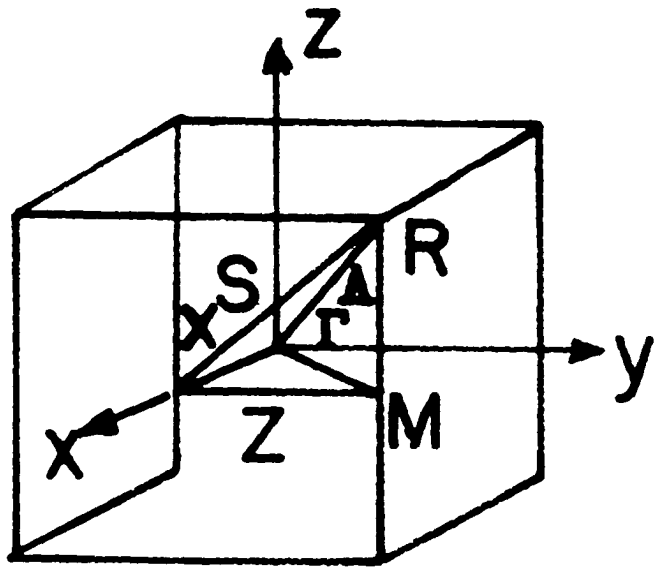

Figure 3. Brillouin zone for the simple cubic bravais lattice, showing high symmetry points and directions.

units is given by

$$V^{\alpha}(|\vec{r} - \vec{r}_j|) = \frac{2Z_{\alpha}}{|\vec{r} - \vec{r}_j|} - U_o^{\alpha}(|\vec{r} - \vec{r}_j|) + 6\left(\frac{3}{8\pi}\rho^{\alpha}(|\vec{r} - \vec{r}_j|)\right)^{1/3} \quad (7)$$

where α denotes different atomic species within the unit cell. The first term in Equation 7 is the nuclear term, the second term is the solution of Poisson's equation, Equation 6, and the last term is the exchange contribution to the potential which is approximated by the Slater (22) exchange term.

The total crystal potential is calculated by summing directly the contributions from the neighboring rhenium and oxygen atoms. This sum is carried out by the Löwdin (23) alpha expansion. Using only the spherically symmetric part of the Löwdin expansion, since we are considering the crystal potential as spherically symmetric, the contribution to the potential of the ith atom in the unit cell due to the potential $V^{\alpha}(|\vec{r} - \vec{r}_j|$ is given by

$$V_j^{\alpha}(|\vec{r} - \vec{r}_i|) = \frac{1}{2d|\vec{r} - \vec{r}_i|}\int_{d - |\vec{r} - \vec{r}_i|}^{d + |\vec{r} - \vec{r}_i|} |\vec{r} - \vec{r}_j| V^{\alpha}(|\vec{r} - \vec{r}_j|)dr_j \quad (8)$$

where $d = |\vec{r}_j - \vec{r}_i|$ is the distance between the ith and jth atoms. Thus the crystal potential about any atom in the unit cell is

$$V_c^{\alpha}(|\vec{r} - \vec{r}_i|) = V^{\alpha}(|\vec{r} - \vec{r}_i|) + \sum_{j=\text{neighbors}} V_j^{\alpha}(|\vec{r} - \vec{r}_i|). \quad (9)$$

When $\alpha = 1$ we are summing about the rhenium sites and when $\alpha = 2$ about

the oxygen sites. The number of neighbors and their distance from the rhenium and oxygen atoms are given in Tables 1 and 2 respectively.

For crystals with one atom per unit cell the value of the potential in the interstitial region is determined by a spherical average. The average potential is given by

$$\bar{V} = \frac{3\int_{R_{MT}}^{R_{WS}} r^2 V(r)\, dr}{R_{WS}^3 - R_{MT}^3} \tag{10}$$

where R_{MT} and R_{WS} are the muffin tin (MT) and Wigner Seitz (WS) radii respectively.

For the case of rhenium trioxide there are four MT radii so to a first approximation the average potential may be given as

$$\bar{V} = 1/4 \sum_i \bar{V}_i \tag{11}$$

where

$$\bar{V}_i = \frac{3\int_{R_{MT_i}}^{R_{WS_i}} |\vec{r} - \vec{r}_i|^2 V(|\vec{r} - \vec{r}_i|)\, dr}{R_{WS_i}^3 - R_{MT_i}^3} \quad . \tag{12}$$

Numerical integration gives $\bar{V}_1 = -2.177$ rydbergs and $\bar{V}_2 = -1.965$ rydbergs; then employing the previously cited approximation to the average potential we find that $\bar{V} = -2.01$ rydbergs.

In order to calculate the spherically averaged potential in the interstitial region using Equation 12, we must know the values of the WS radii for each atomic species. These radii must be defined so that

Table 1. Distances of neighbor atoms from rhenium

Shell number	Type of atom	Number of atoms per shell	Distance from rhenium in units of the lattice constant
1	Oxygen (O)	6	1/2
2	Rhenium (Re)	6	1
3	O	24	$\sqrt{5}/2$
4	Re	12	$\sqrt{2}$
5	O	30	3/2
6	Re	8	$\sqrt{3}$
7	O	24	$1/2\sqrt{13}$
8	Re	8	2
9	O	48	$\sqrt{17}/2$
10	Re	24	$\sqrt{5}$
11	O	48	$\sqrt{21}/2$
12	Re	24	$\sqrt{6}$
13	O	30	5/2
14	O	72	$\sqrt{29}/2$
15	Re	12	$\sqrt{8}$
16	O	96	$\sqrt{33}/2$
17	Re	30	3

Table 2. Distances of neighbor atoms from oxygen

Shell number	Type of atom	Number of atoms per shell	Distance from oxygen in units of the lattice constant
1	Rhenium (Re)	2	1/2
2	Oxygen (O)	8	$\sqrt{2}/2$
3	O	6	1
4	Re	8	$\sqrt{5}/2$
5	O	16	$\sqrt{6}/2$
6	O	12	$\sqrt{2}$
7	Re	10	3/2
8	O	12	$\sqrt{10}/2$
9	O	8	$\sqrt{3}$
10	Re	8	$\sqrt{13}/2$
11	O	32	$\sqrt{14}/2$
12	O	6	2
13	Re	16	$\sqrt{17}/2$
14	O	24	$\sqrt{18}/2$
15	O	24	$\sqrt{5}/2$
16	Re	16	$\sqrt{21}/2$

the volume occupied by the sum of all the "Wigner Seitz cells" is equal to the volume of the unit cell. Constructing such a set of radii is of course possible, but the averaged interstitial potential using the previously outlined scheme yields a value for the potential in this region which is incorrect. This can be shown by the following arguments.

Figure 4 shows a two dimensional unit cell with two different atomic species. The muffin tin radii are drawn so that they are touching; this insures that the largest amount of charge of an atomic species is contained inside the MT radii. The WS radii are drawn so that the volume occupied by the sum of all the "Wigner Seitz cells" is equal to the volume of the unit cell. If this is the case, then the WS radius of an atom will enter inside the MT region of a neighboring atom. Then there will be a contribution to the average interstitial potential which is not due to anything in the interstitial region, but rather by the potential inside the MT radius of a neighboring atom. This clearly gives an average value to the potential in this region which is larger than its true magnitude. A method different from the standard method of averaging the interstitial potential is therefore needed.

The average potential in the interstitial region is rigorously defined as

$$V_{AV} = \frac{\int_{INT} V(r)\, d^3r}{V_{INT}} \tag{13}$$

where V_{INT} is the volume of the interstitial region. The potential

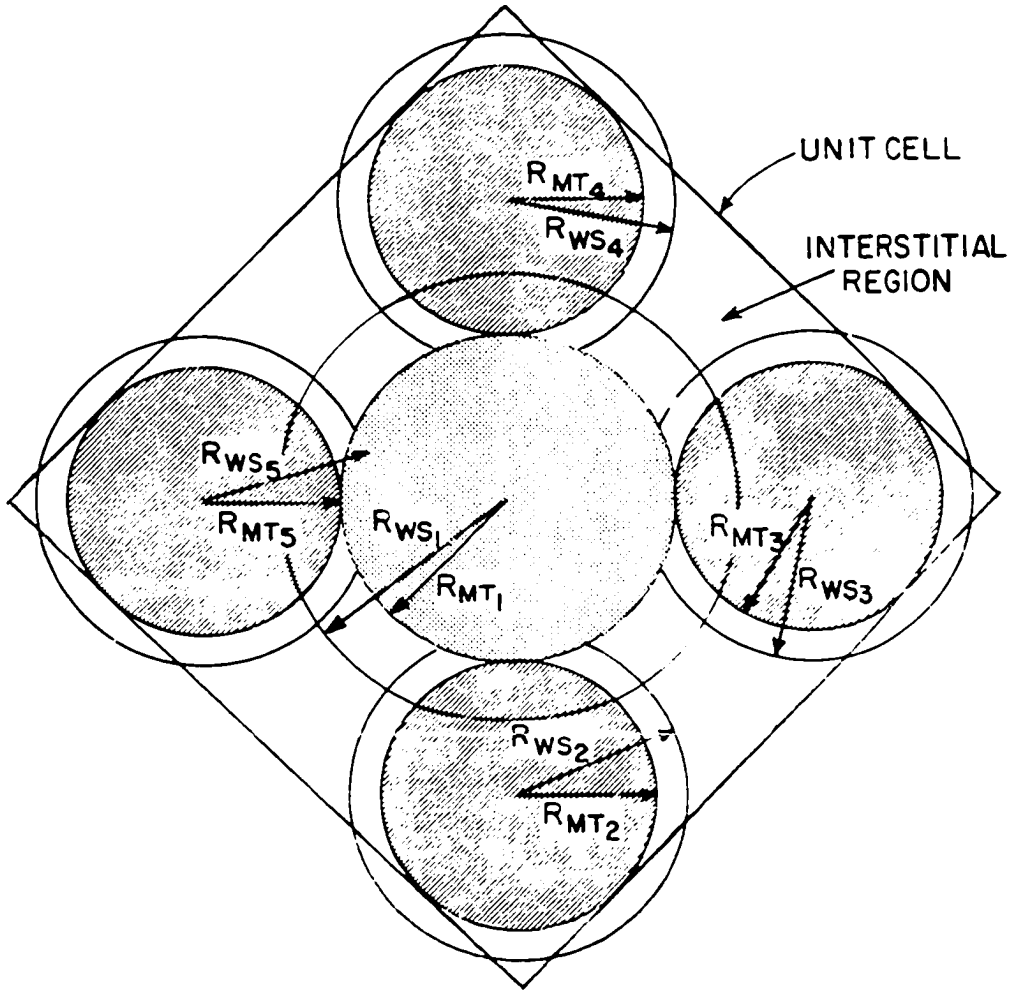

Figure 4. A unit cell in two dimensions with two different atomic species. The muffin tin and Wigner Seitz radii are shown.

V(r) may be written as

$$V(r) = \sum_{K \neq 0} V(K)\, e^{i\vec{K} \cdot \vec{r}} \tag{14}$$

where V(K) is the Fourier transform of the potential. Substituting Equation 14 into 13 we get

$$V_{AV} = \frac{1}{V_{INT}} \sum_{K \neq 0} V(K) \int_{(INT)} e^{i\vec{K} \cdot \vec{r}}\, d^3r. \tag{15}$$

If a function $f(\vec{r})$ is periodic with respect to a lattice translation then

$$\int_{\text{unit cell}} d^3r\, f(\vec{r})\, e^{i\vec{K} \cdot \vec{r}} = 0 ,$$

and then the integral in Equation 15 may be written as

$$\int_{(INT)} e^{i\vec{K} \cdot \vec{r}}\, d^3r = - \int_{(\text{muffin tins})} e^{i\vec{K} \cdot \vec{r}}\, d^3r.$$

Then Equation 15 may also be written as

$$V_{AV} = - \frac{1}{V_{INT}} \sum_{K \neq 0} V(K) \int_{(\text{muffin tins})} e^{i\vec{K} \cdot \vec{r}}\, d^3r. \tag{16}$$

If we represent the position of the νth atom in the unit cell as $\vec{r}_\nu$ then

$$\int_{\substack{\text{muffin}\\\text{tins}}} e^{i\vec{K}\cdot\vec{r}}\, d^3r = \sum_\nu e^{i\vec{K}\cdot\vec{r}_\nu} \int_{\substack{\nu\text{muffin}\\\text{tins}}} e^{i\vec{K}\cdot(\vec{r}-\vec{r}_\nu)}\, d^3r$$

$$= \sum_\nu e^{i\vec{K}\cdot\vec{r}_\nu}\, G(Kr_{MT}^{\nu}) \ .$$

The function $G(x) = 3/x^3(\sin x - x\cos x)$ is the Fourier transform of a three dimensional step function and r_{MT}^{ν} is the MT radius of the νth atom. The integral expression of $G(x)$ is shown by Ziman (24) but can be done quite easily if we let $\vec{r}' = \vec{r} - \vec{r}_\nu$. Finally Equation 16 may be written as

$$V_{AV} = -\frac{1}{V_{INT}} \sum_{K\neq 0} V(K) \sum_\nu e^{i\vec{K}\cdot\vec{r}_\nu}\, G(Kr_{MT}^{\nu}) \tag{17}$$

where $V(K)$ is defined by Equation 14 and

$$V(K) = -\frac{8\pi}{\Omega K^2}\left[\sum_\nu Z_\nu\, G(Kr_{MT}^{\nu}) - \left[\rho_\nu(k) + 6\left(\frac{3}{8\pi}\rho_\nu(k)\right)^{1/3}\right] x\right.$$

$$\left. e^{-i\vec{K}\cdot\vec{r}_\nu}\right]. \tag{18}$$

The terms in Equation 18 are the Fourier transforms of the nuclear, Coulomb and Slater exchange contributions to the potential respectively.

The value of the potential in the interstitial region is then calculated numerically using Equations 17 and 18 and its value is -.811 rydbergs. This value is more than half as much as the previously quoted value and is consistent with the previous discussion of the

interstitial potential.

The Muffin Tin Radii

In metals with one atom per unit cell the muffin tin (MT) radii are chosen as large as possible so that twice the MT radius is equal to the nearest neighbor distance. Thus the ratio of all MT radii will obviously be unity, since all the atoms in this crystal are identical. In the case of rhenium trioxide it is not immediately obvious how the MT radii should be weighted so that the sum of the radii is equal to the nearest neighbor distance.

Mattheiss' (10,11) reason for choosing the ratio of the MT radii, $\frac{R(\text{rhenium})}{R(\text{oxygen})}=7/6$, is not transparent. However, it is plausible that the ratio was chosen from the number of conduction electrons in rhenium, five 5d and two 6s electrons, to the number in oxygen, two 2s and four 2p electrons. Weighting the MT radii to be equal to the ratio of conduction electrons in each atomic species seems to be inadequate for the following reason. Tightly bound electron states cannot be approximated well by a plane wave expansion in the interstitial region. These electrons must be inside the MT radii. It is unnecessary for electrons which are not tightly bound to be entirely within the MT radii, since these electron states can be approximated reasonably well by a combination of plane waves in the interstitial region. Weighting the MT radii by the number of conduction electrons does not guarantee that the d electrons will not be in the interstitial region.

In choosing the MT radii for this calculation we have plotted the number of electrons, $n_\ell = 4\pi\int_0^\infty r^2 \rho_\ell(r)dr$, for a given angular momentum

as a function of distance from the nucleus. This is shown in Figure 5. The broken curve represents the number of $5d^5$ electrons of rhenium and the two unbroken curves represent the $2s^2$ and $2p^4$ electrons of oxygen within a given shell of radius r. The MT radius of rhenium should be chosen so that the largest possible amount of electronic charge is inside this radius. Mattheiss' choice of R_{MT} of rhenium gives 3.3 electrons inside the MT sphere while our choice is larger and includes 3.8 electrons inside.

Ideally we should choose the radius of rhenium to be even larger, but then the corresponding oxygen radii would decrease and more oxygen s and p electrons would be outside the MT sphere. Thus in order to represent these s and p wave functions faithfully in the interstitial region, more plane waves would have to be added to the formalism. This would be computationally prohibitive since the secular determinant's order would increase by 50% for one additional angular momentum state. Therefore we have increased the MT radius of rhenium from the value quoted by Mattheiss so that the MT sphere can hold more d-like charge and also increased the number of angular momentum states of oxygen to $\ell = 2$ in order to represent the s and p electrons of oxygen more accurately away from an oxygen state.

In order to perform a realistic calculation of the electronic states of a crystal under pressure, the lattice parameter as a function of pressure is required. Schirber *et al.* (15) provided the bulk compressibility, $K = (5.3 \pm .9) \times 10^{-4}$/kbar, of ReO_3 at 24°C. Assuming that the value of K remains linear at high pressure, then the change in

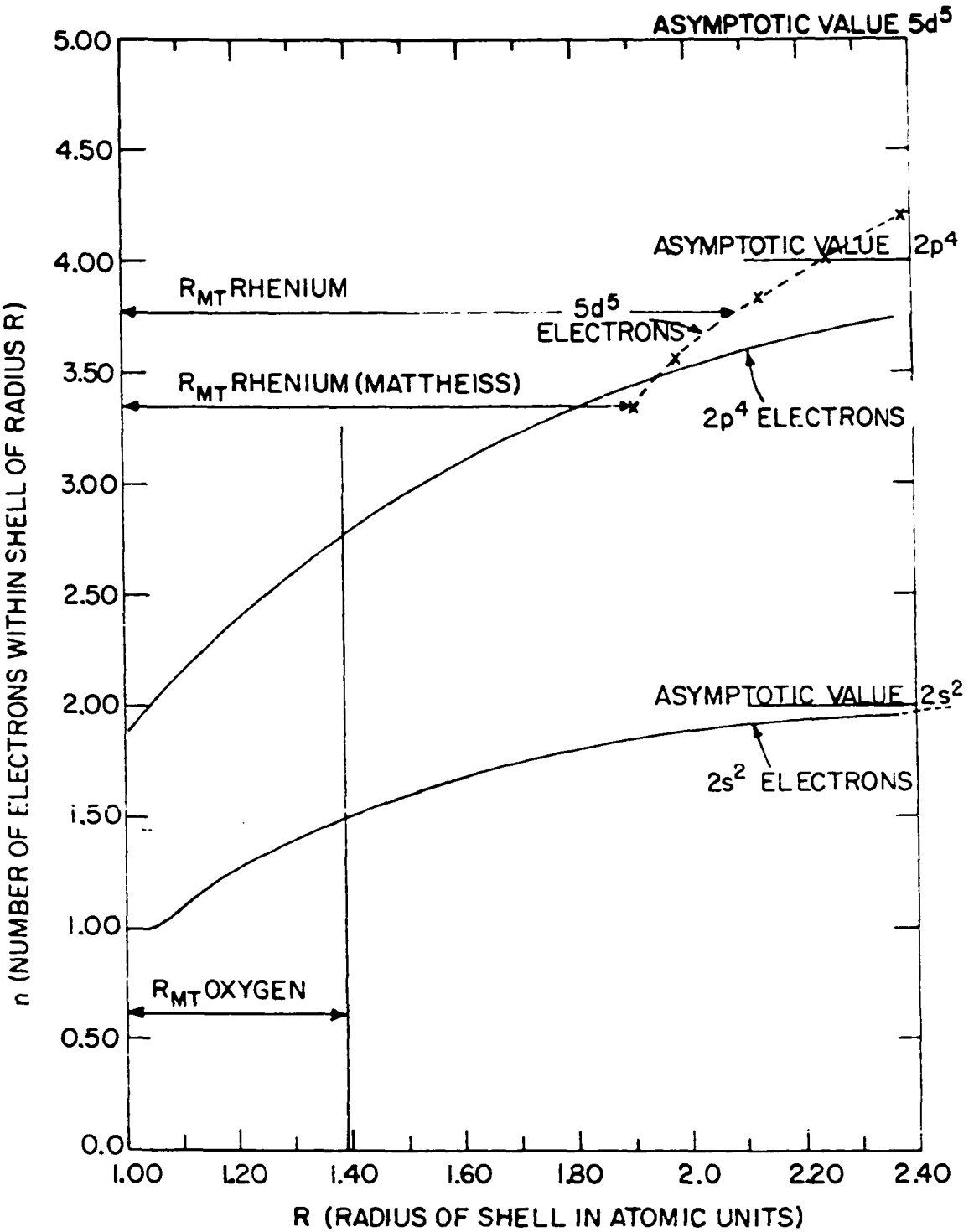

Figure 5. Number of electrons for certain angular momentum as a function of distance from the nuclei.

the lattice parameter as a function of pressure is given by da = -1/3 Kadp where da is the change in the lattice parameter and dp is the change in the pressure. The values of the lattice parameters and the muffin tin sphere radii for the equilibrium lattice constant and the 2% compressed lattice constant are given in Table 3.

Table 3. Parameters used in calculating electronic energy bands.

Pressure kbar	Lattice parameter (au)	MT radii Rhenium (au)	Oxygen (au)
0	7.0705	2.0834	1.3994
113	6.9290	1.9740	1.3911

KKR METHOD

The Green's Function Method

The Green's function method for the solution of the Schroedinger equation in periodic lattices was developed independently by Korringa (17) and Kohn and Rostoker (18). This method is commonly called the KKR method.

The Schroedinger equation for a particle in a periodic potential $V(\vec{r})$ is

$$(-\nabla^2 + V(\vec{r}) - E)\psi(\vec{r}) = 0 . \tag{19}$$

The solutions to Equation 19 satisfy the following boundary conditions in the central polyhedron surrounding the origin:

$$\psi(\vec{r} + \vec{r}_s) = e^{i\vec{k} \cdot \vec{r}_s} \psi(\vec{r})$$

and

$$\left.\frac{\partial\psi(\vec{r} + \vec{r}_s)}{\partial(\vec{r} + \vec{r}_s)}\right]_n = - e^{i\vec{k} \cdot \vec{r}_s} \left.\frac{\partial\psi(\vec{r})}{\partial r}\right]_n .$$

Kohn and Rostoker have shown that a solution for Equation 19 is

$$\psi(\vec{r}) = \int G(\vec{r},\vec{r}')V(\vec{r}')\psi(\vec{r}')d^3\vec{r}' \tag{20}$$

where $V(\vec{r}')$ and $\psi(\vec{r}')$ are respectively the scattering potential and the

wave function within this potential. The Green's function $G(\vec{r},\vec{r}')$ connects $\psi(\vec{r})$ to $\psi(\vec{r}')$ and conversely.

Rewriting Equation 19 and substituting the value of $\psi(\vec{r})$ from Equation 20 into Equation 19 we get

$$V(\vec{r})\psi(\vec{r}) = \int(\nabla^2 + E)G(\vec{r},\vec{r}')V(\vec{r}')\psi(\vec{r}')d^3\vec{r}' \quad . \tag{21}$$

If

$$(\nabla^2 + E)G(\vec{r},\vec{r}') = \delta(\vec{r} - \vec{r}') \tag{22}$$

then Equation 21 is satisfied. From Equation 20 $G(\vec{r},\vec{r}')$ must also satisfy the same boundary conditions as the solutions to Equation 19.

From Jackson (25), the Green's function can be expanded in a series of free particle eigenfunctions of the form

$$G(\vec{r},\vec{r}') = \sum_n a_n(\vec{r}')\psi_n(\vec{r}) \tag{23}$$

where n sums over the reciprocal lattice vectors. Substituting Equation 23 into Equation 22 we get

$$\sum_n a_n(\vec{r}')[-(\vec{K}_n + \vec{k})^2 + E]\ \psi_n(\vec{r}) = \delta(\vec{r} - \vec{r}') \tag{24}$$

since

$$\psi_n(\vec{r}) = \frac{1}{\sqrt{\tau}} \exp i(\vec{K}_n + \vec{k}) \cdot \vec{r} \tag{25}$$

where τ is the volume of the atomic polyhedron and $\vec{k}$ is any point in the Brillouin zone. If we multiply both sides of Equation 24 by $\psi_m^*(\vec{r})$ and integrate over solid angle we find

$$a_n(\vec{r}') = \frac{\psi_n^*(\vec{r}')}{E - (\vec{K}_n + \vec{k})^2} \tag{26}$$

and

$$G(\vec{r},\vec{r}') = -\frac{1}{\tau} \sum_n \frac{\exp i(\vec{K}_n + \vec{k}) \cdot (\vec{r} - \vec{r}')}{(\vec{K}_n + \vec{k})^2 - E} \tag{27}$$

when Equations 25 and 26 are substituted into Equation 23. This is the standard expansion of the Green's function in terms of the eigenfunctions of the homogeneous boundary value problem.

Equation 27 may be expanded in the form

$$G(\vec{r},\vec{r}') = \sum_{\ell m} \sum_{\ell' m'} [A_{\ell m;\ell' m'} j_\ell(Kr) j_{\ell'}(Kr') + \\ + K\delta_{\ell\ell'}\delta_{mm'} j_\ell(Kr)\eta_\ell(Kr')] Y_{\ell m}(\hat{r}) Y_{\ell' m'}^*(\hat{r}') \quad \text{for } r < r' \tag{28}$$

where $K = \sqrt{E}$ for $E > 0$ and $K = i\sqrt{-E}$ for $E < 0$. $j_\ell(x)$ and $\eta_\ell(x)$ are spherical Bessel functions and the structure constants $A_{\ell m,\ell' m'}$ are fixed functions of E and $\vec{k}$ for a characteristic lattice, except for

scaling factors.

In order to find an expression for these structure constants, we must use the plane wave expansion on Equation 27. The plane wave expansion is

$$e^{i\vec{K}\cdot\vec{R}} = 4\pi \sum_{L} \sum_{M=-L}^{+L} i^{L} j_{L}(KR) Y_{LM}(\hat{R}) Y_{LM}^{*}(\hat{K}). \tag{29}$$

Expanding $e^{i(\vec{K}_n + \vec{k})\cdot\vec{r}}$ and $e^{-i(\vec{K}_n + \vec{k})\cdot\vec{r}'}$ by Equation 29 and substituting into Equation 27 we get

$$G(\vec{r},\vec{r}') = -\frac{(4\pi)^2}{\tau} \sum_{L,M} \sum_{L',M'} i^{L-L'} \times \tag{30}$$

$$\frac{j_L(|\vec{K}_n+\vec{k}|r) j_{L'}(|\vec{K}_n+\vec{k}|r') Y_{LM}(\hat{r}) Y_{L'M'}^{*}(\hat{r}') Y_{LM}^{*}(\hat{K}_n+\hat{k}) Y_{L'M'}(\hat{K}_n+\hat{k})}{(\vec{K}_n+\vec{k})^2 - E}$$

If we define a quantity $D(\vec{r},\vec{r}')$ as

$$D(\vec{r},\vec{r}') = G(\vec{r},\vec{r}') - G_o(\vec{r},\vec{r}') \tag{31}$$

where

$$G_o(\vec{r},\vec{r}') = -\frac{1}{4\pi} \frac{\cos K(|\vec{r} - \vec{r}'|)}{|\vec{r} - \vec{r}'|} \tag{32}$$

$$= \begin{cases} K \sum_{\ell,m} j_\ell(Kr)\, \eta_\ell(Kr') Y_{\ell m}(\hat{r}) Y_{\ell' m'}^{*}(\hat{r}') & \text{for } r < r' \\ K \sum_{\ell,m} j_\ell(Kr') \eta_\ell(Kr) Y_{\ell m}^{*}(\hat{r}') Y_{\ell' m'}(\hat{r}) & \text{for } r' < r \end{cases}$$

then $(\nabla^2 + E)D(\vec{r},\vec{r}') = 0$, since $(\nabla^2 + E)G_o(\vec{r},\vec{r}') = \delta(\vec{r} - \vec{r}')$. Consequently $D(\vec{r},\vec{r}')$ satisfies the homogenous wave equation and for $r < R_{\text{muffin tin}}$, a general solution of the homogeneous equation for $D(\vec{r},\vec{r}')$ has the form

$$D(\vec{r},\vec{r}') = \sum_{\ell,m} \sum_{\ell',m'} A_{\ell m;\ell' m'}\, j_\ell(Kr) j_{\ell'}(Kr') Y_{\ell m}(\hat{r}) Y^*_{\ell' m'}(\hat{r}') \qquad (33)$$

for $r < r'$. Together with Equation 33, 31, and 32, the Green's function given by Equation 27 becomes

$$G(\vec{r},\vec{r}') = \sum_{\ell,m} \sum_{\ell',m'} [A_{\ell m;\ell' m'} j_\ell(Kr) j_{\ell'}(Kr') + K\delta_{\ell\ell'}\delta_{mm'} j_\ell(Kr)\eta_\ell(Kr')] \times$$

$$Y_{\ell m}(\hat{r}) Y^*_{\ell' m'}(\hat{r}')$$

which is the expansion of the Green's function as previously cited.

To find an expression for the structure constants, equate Equations 30 and 28, multiply by $Y^*_{\ell,m}(\hat{r}) Y_{\ell',m'}(\hat{r}')$ and integrate over solid angle to get

$$A_{\ell m;\ell' m'} = -\frac{(4\pi)^2\, i^{\ell-\ell'}}{\tau\, j_\ell(Kr) j_{\ell'}(Kr')} \times \qquad (34)$$

$$\sum_n \frac{j_\ell(|\vec{K}_n+\vec{k}|r) j_{\ell'}(|\vec{K}_n+\vec{k}|r') Y_{\ell m}(\hat{\vec{K}}_n+\vec{k}) Y^*_{\ell' m'}(\hat{\vec{K}}_n+\vec{k})}{(\vec{K}_n+\vec{k})^2 - E}$$

$$- K\delta_{\ell\ell'}\delta_{mm'} \frac{\eta_\ell(Kr')}{j_\ell(Kr')}$$

for $r < r' < R_{\text{muffin tin}}$. The structure constants are the same for any pair of $\vec{r}$ and $\vec{r}'$.

As mentioned previously, the structure constants are functions of energy and position in the Brillouin zone only. These constants, once calculated and stored, may be used over on any crystal which has the same lattice.

The Variational Expression for Energy

If we define a quantity Λ as

$$\Lambda \equiv \int_r \psi^*(\vec{r})V(\vec{r})\psi(\vec{r})d^3r \tag{35}$$

$$- \int_r \int_{r'} \psi^*(\vec{r})V(\vec{r})G(\vec{r},\vec{r}')V(\vec{r}')\psi(\vec{r}')d^3r d^3r'$$

and vary Λ with respect to $\psi^*(\vec{r})$ and set

$$\delta\Lambda = 0 \tag{36}$$

we get the integral definition of the wave function, Equation 20. According to the previously cited work of Kohn and Rostoker Λ is the variational function. In order to evaluate Λ it is necessary to transform the expression for Λ from volume to surface integrals. This may be done with the aid of Green's Theorem

$$\int (U\nabla^2 V - V\nabla^2 U)d^3r = \int (U \text{ grad } V - V \text{ grad } U) \cdot d\vec{s} \ . \tag{37}$$

We let $U = G(\vec{r},\vec{r}')$, $V = \psi(\vec{r}')$ and let $\vec{r} \to \vec{r}'$ and substitute back into Equation 37 to get

$$\int (G(\vec{r},\vec{r}')\nabla'^2\psi(\vec{r}')-\psi(\vec{r}')\nabla'^2 G(\vec{r},\vec{r}'))d^3r'$$

$$= \int (G(\vec{r},\vec{r}')\text{grad}'\psi(\vec{r}')-\psi(\vec{r}')\text{grad}'G(\vec{r},\vec{r}')) \cdot d\vec{s}' \ . \tag{38}$$

If we now add $-\int EG(\vec{r},\vec{r}')d^3r$ to both sides of Equation 38 and using Equations 19 and 22 when $\vec{r} \to \vec{r}'$ we get the following:

$$\psi(\vec{r})-\int G(\vec{r},\vec{r}')V(\vec{r}')\psi(\vec{r}')d^3r'$$

$$= \int (\psi(\vec{r}')\text{grad}'G(\vec{r},\vec{r}')-G(\vec{r},\vec{r}')\text{grad}'\psi(\vec{r}')) \cdot d\vec{s}'. \tag{39}$$

Now if we consider the expression

$$\int d^3r\psi^*(\vec{r})V(\vec{r})G(\vec{r},\vec{r}') = \int d^3r(\nabla^2+E)\psi^*(\vec{r})G(\vec{r},\vec{r}') \tag{40}$$

and apply Green's Theorem and Equation 22 we get

$$\int d^3r\psi^*(\vec{r})V(\vec{r})G(\vec{r},\vec{r}) = \int (G(\vec{r},\vec{r}')\text{grad}\psi^*(\vec{r})-\psi^*(\vec{r})\text{grad}G(\vec{r},\vec{r}')) \cdot d\vec{s}. \tag{41}$$

Finally rewriting Λ as

$$\Lambda = \lim_{\epsilon \to 0} \Lambda_\epsilon = \int_{r<R_i-2\epsilon} d^3r\psi^*(r)V(r) \times$$

$$[\psi(\vec{r})-\int_{r'<R_i-\epsilon} d^3r' G(\vec{r},\vec{r}')V(\vec{r}')\psi(\vec{r}')]$$

and substituting Equations 39 and 41 into this expression for Λ we get

$$\Lambda = \lim_{\epsilon \to 0} \Lambda_\epsilon = \int_{S(R_i-2\epsilon)} ds \int_{S'(r_i-\epsilon)} ds' \left(\frac{\partial \psi^*(\vec{r})}{\partial r} - \psi^*(\vec{r}) \frac{\partial}{\partial r} \right) \times \left(\psi(\vec{r}') \frac{\partial}{\partial r'} G(\vec{r},\vec{r}') - G(\vec{r},\vec{r}') \frac{\partial}{\partial r'} \psi(\vec{r}') \right), \tag{42}$$

where R_i is the muffin tin radius. Equation 42 implicitly assumes that the interstitial potential is constant.

Using a trial wave function

$$\psi(\vec{r}) = \sum_{i=0}^{n} C_i \phi_i \tag{43}$$

and substituting $\psi(\vec{r})$ into the expression for Λ, we get

$$\Lambda = \sum_{i,j=0}^{n} C_i^* C_j \Lambda_{i,j} \tag{44}$$

where $\Lambda_{i,j}$ is Hermitian and is defined as

$$\Lambda_{ij} = \int_r \phi_i^*(\vec{r}) V(\vec{r}) \phi_j(\vec{r}) d^3r - \int_r \int_{r'} \phi_i^*(\vec{r}) V(\vec{r}) G(\vec{r},\vec{r}') V(\vec{r}') \phi_j(\vec{r}') d^3r d^3r'. \tag{45}$$

The condition $\frac{\partial \Lambda}{\partial C_i} = 0$ follows from Equation 36, and yields the linear equations

$$\sum_j \Lambda_{ij} C_j = 0, \quad i = 0,1,\ldots,n \tag{46}$$

From the theory of linear equations, we know that a homogeneous system of n equations in the same number of unknowns has nontrivial solutions if, and only if, the determinant of its coefficients is zero. The equation

$$\det \Lambda_{i,j} = 0 \tag{47}$$

then determines the stationary energy eigenvalues as a function of $\vec{k}$.

Simplifications for Spherically Symmetric Potentials

As previously discussed, the crystal potential or muffin tin potential is spherically symmetric within a muffin tin radius and equal to zero in the interstitial region. If $V(\vec{r})$ is spherically symmetric then

$$V(\vec{r}) = \begin{cases} V(|\vec{r}|) & \text{for } |\vec{r}| \leq R_i \\ 0 & \text{otherwise} \end{cases} \tag{48}$$

where R_i is the muffin tin radius.

For this class of potentials the trial wave function is

$$\phi = \sum_{\ell=0}^{\ell_{max}} \sum_{m=-\ell}^{+\ell} C_{\ell m} R_\ell(|\vec{r}|) Y_{\ell m}(\hat{r}) \quad \text{for } r \leq R_i \tag{49}$$

where $R_\ell(|\vec{r}|)$ is defined as

$$\left(\frac{1}{r^2}\frac{d}{dr}r^2\frac{d}{dr} + \frac{\ell(\ell+1)}{r^2} + V(|\vec{r}|) - E\right)R_\ell(|\vec{r}|) = 0 \tag{50}$$

Substituting the value of the Green's function, Equation 28, and the trial wave function, Equation 49, into the variational expression for energy, Equation 45, and taking the limit $\epsilon \to 0$, then the matrix elements of Λ are given by

$$\Lambda_{\ell m;\ell' m'} = (L_\ell j_\ell - j_{\ell'})[(A_{\ell m;\ell' m'} j'_{\ell'} + K\delta_{\ell\ell'}\delta_{mm'}\eta'_{\ell'}) - (A_{\ell m;\ell' m'} j_{\ell'} + K\delta_{\ell\ell'}\delta_{mm'}\eta_{\ell'})L_{\ell'}], \tag{51}$$

where

$$L_\ell = \frac{1}{R_\ell(r)}\frac{dR_\ell(r)}{dr}\Bigg|_{r = R_i}.$$

Dividing each row of the matrix by $(L_\ell j_\ell - j_\ell')$ and each column by $(L_{\ell'} j_{\ell'} - j'_{\ell'})$ and setting the determinant equal to zero, according to Equation 47, we obtain the stationary energy eigenvalues as a function of $\vec{k}$ when

$$\text{Det}\left|A_{\ell m;\ell' m'} + K\delta_{\ell\ell'}\delta_{mm'}\frac{\eta_\ell' - \eta_\ell L_\ell}{j_\ell' - j_\ell L_\ell}\right| = 0. \tag{52}$$

This result of the KKR method enables us to calculate the electronic energy states of a crystal which has one atom per unit cell. However,

the present calculation of ReO_3 requires some modifications of the Green's function method which will be shown in the next section.

The KKR Method for "Complex Crystals"

Following the work of Korringa, Kohn and Rostoker, Segall(16) developed a method which calculates the electronic energy states of "complex crystals". A "complex crystal" for this work is one which has more than one atom per unit cell. Segall's theory, when applied, can determine the band structure of compounds, which up to that time could not be ascertained by simple KKR.

Segall's variational expression for energy is given by

$$\Lambda = \lim_{\epsilon \to 0} \Lambda_\epsilon \tag{53}$$

$$= [S_{1,2\epsilon} + \cdots + S_{n,2\epsilon}][S_{1,\epsilon} + \cdots + S_{n,\epsilon}]$$

where

$$S_{1,2\epsilon} = \int_{S_{n(R-2\epsilon)}} d\vec{S} \cdot [\psi_1^*(\vec{r}) \frac{\partial}{\partial r} - \frac{\partial}{\partial r} \psi_1^*(\vec{r})]$$

and

$$S_{1,\epsilon} = \int_{Sn(R-\epsilon)} d\vec{S}' \cdot [G(\vec{r},\vec{r}') \frac{\partial}{\partial r'} \psi_1(\vec{r}') - \psi_1(\vec{r}') \frac{\partial}{\partial r'} G(\vec{r},\vec{r}')].$$

Equation 53 is a product of sums of surface integrals. The ith atom in the unit cell has contributions in Λ with every other atom in the

unit cell and also a self interaction. These self interactions $(S_{i,2\epsilon})(S_{i,\epsilon})$ are simply the variational expressions as given by Kohn and Rostoker. The trial wave function in this case is given by

$$\psi(\vec{r}) = \sum_{\ell=0}^{\ell_{max}} \sum_{m=-\ell}^{+\ell} C_{\ell m}{}^{(j)} R_{\ell}{}^{(j)}(|\vec{r}-\vec{a}_j|) Y_{\ell m}(\hat{\vec{r}-\vec{a}_j}), \quad |\vec{r}-\vec{a}_j| \leq R_j \tag{54}$$

The vector $\vec{a}_j$ is the position vector of the jth atom with respect to the origin. If we now define a vector $\vec{r}_j$ to be the position vector with respect to the jth atom in the unit cell, then

$$\vec{r}_j = \vec{r}-\vec{a}_j \text{ and } \vec{r}'_{j'} = \vec{r}'-\vec{a}_{j'}. \tag{55}$$

The Green's function which connects the jth atom to the j'th atom is defined as

$$G^{(j,j')}(\vec{r}_j,\vec{r}'_{j'}) = G(\vec{r},\vec{r}') = G(\vec{r}_j-\vec{r}'_{j'}-(\vec{a}_{j'}-\vec{a}_j)) \tag{56}$$

where $G(\vec{r},\vec{r}')$ is given by Equation 27, then

$$G^{(j,j')}(r_j,r'_{j'}) = -\frac{1}{\tau}\sum_n \frac{\exp i(\vec{K}_n+\vec{k})\cdot(\vec{a}_j-\vec{a}_{j'})\exp i(\vec{K}_n+\vec{k})\cdot(\vec{r}_j-\vec{r}'_{j'})}{(\vec{K}_n+\vec{k})^2 - E} \tag{57}$$

Just as before the Green's function may be expanded as

$$G^{(j,j')}(r_j,r'_{j'}) = \sum_{\ell,m}\sum_{\ell',m'} A^{(j,j')}_{\ell m;\ell' m'} j_{\ell'}(Kr_j) j_{\ell'}(Kr'_j) Y_{\ell m}(\hat{r}_j) Y^{*}_{\ell m}(\hat{r}'_{j'}) \tag{58}$$

for $(\vec{r}_j+\vec{r}'_{j'}) < |\vec{a}_j-\vec{a}_{j'}|$.

Using the plane wave expansion on Equation 57, equating Equations 57 and 58, multiplying by $Y^*_{LM}(\hat{r}_j)Y_{LM}(\hat{r}'_{j'})$ and integrating over solid angle, we find that the nondiagonal structure constants are given by

$$A^{(j,j')}_{\ell m;\ell' m'} = -\frac{(4\pi)^2 i^{\ell-\ell'}}{\tau\, j_\ell(Kr_j) j_{\ell'}(Kr'_{j'})} \sum_n \frac{\exp i(\vec{K}_n+\vec{k})\cdot\vec{a}_j-\vec{a}_{j'})}{(\vec{K}_n+\vec{k})^2 - E} \times \tag{59}$$

$$j_\ell(|\vec{K}_n+\vec{k}|r_j) j_{\ell'}(|\vec{K}_n+\vec{k}|r'_{j'}) Y^*_{\ell m}(\hat{\vec{K}}_n+\vec{k}) Y_{\ell' m'}(\hat{\vec{K}}_n+\vec{k}).$$

Following the procedure outlined in previous sections, the stationary energy eigenvalues as a function of $\vec{k}$ for a "complex crystal" are given by

$$\text{Det}\left| A^{(j,j')}_{\ell m;\ell' m'} + K\delta_{jj'}\delta_{\ell\ell'}\delta_{mm'} \left.\frac{\eta_{\ell'} - \eta_\ell L_\ell(j)}{j_{\ell'} - j_\ell L_\ell(j)}\right|_{r=R_j} \right| = 0.$$

The expression in Equation 59 is a perfectly valid expression for the values of the structure constants. However when these expressions are evaluated numerically, even with the use of a high speed computer, the convergence of the quantities is very slow indeed. It therefore becomes necessary to split up the Green's function into a sum over real and reciprocal space. This is done with the aid of a procedure developed by Ewald (26) and will be shown in the next section.

Alternative Definition for the Structure Constants

The Green's function given by Equation 57 is a sum over reciprocal lattice vectors. In order to transform the Green's function into a

sum over real and reciprocal lattice vectors, it is necessary to transform Equation 57 into a sum over real space vectors.

Equation 57 may be transformed into an expression which only depends on one vector, $\vec{R}_{jj'}$, if we let $\vec{R}_{jj'} = \vec{r}_j - \vec{r}_{j'}$ and substitute this into Equation 57 we get

$$G^{(j,j')}(\vec{R}_{jj'}) = + \lim_{\epsilon \to +0} -\frac{1}{\tau}\sum_n \frac{\exp i(\vec{K}_n+\vec{k})\cdot(\vec{R}_{jj'}+\vec{a}_j-\vec{a}_{j'})}{(\vec{K}_n+\vec{k})^2-(E+i\epsilon)} \tag{60}$$

$$= \lim_{\epsilon \to +0} -\frac{1}{\tau}\sum_n \int \frac{\delta(\vec{K}_n+\vec{k}-\vec{K})\exp i(\vec{K}\cdot(\vec{R}_{jj'}+\vec{a}_j-\vec{a}_{j'}))}{K^2-(E+i\epsilon)}\, d\vec{K}.$$

Using the identities

$$\frac{1}{(2\pi)^3}\int e^{i(\vec{K}_n+\vec{k}-\vec{K})\cdot\vec{\rho}}\, d\vec{\rho} = \delta(\vec{K}_n+\vec{k}-\vec{K})$$

and

$$\frac{1}{\tau}\sum_n \exp i(\vec{K}_n\cdot\vec{\rho}) = \sum_S \delta(\vec{\rho}-\vec{r}_s)$$

and substituting these expressions into the last equation we find that

$$G^{(j,j')}(R_{jj'}) = \lim_{\epsilon \to 0+} -\frac{1}{(2\pi)^3}\sum_s \int \frac{\exp i\vec{k}\cdot\vec{r}_s \exp i\vec{K}\cdot(\vec{R}_{jj'}-\vec{r}_s+\vec{a}_j-\vec{a}_{j'})}{K^2-(E+i\epsilon)} d\vec{K}. \tag{61}$$

After integrating, we find that

$$G^{(j,j')}(\vec{R}_{jj'}) = -\frac{1}{4\pi}\sum_s \frac{\exp i\vec{k}\cdot\vec{r}_s \exp i\kappa|\vec{R}_{jj'}-\vec{r}_s+\vec{a}_j-\vec{a}_{j'}|}{|\vec{R}_{jj'}-\vec{r}_s+\vec{a}_j-\vec{a}_{j'}|}, \tag{62}$$

this is the form of the Green's function $G^{(j,j')}(\vec{r}_j,\vec{r}'_j)$ as a sum over the basis vectors of the crystal. Using a relationship derived by Ewald (26)

$$\frac{e^{i\kappa|\vec{R}-\vec{r}_s|}}{|\vec{R}-\vec{r}_s|} = \frac{2}{\sqrt{\pi}}\int_{O(C)}^{\infty} \exp[-(\vec{R}-\vec{r}_s)^2\xi^2+\kappa/4\xi^2]\, d\xi \tag{63}$$

and substituting Equation 63 into 62 we find

$$G^{(j,j')} = -\frac{1}{2\pi^{3/2}}\sum_s e^{i\vec{k}\cdot\vec{r}_s}\int_{O(C)}^{\infty}\exp[-(\vec{r}_{jj'}+\vec{a}_j-\vec{a}_j-\vec{r}_s)^2\xi^2 + \kappa^2/4\xi^2]d\xi. \tag{64}$$

Following the procedure of Ham and Segall (19), who derived the structure constants for one atom per unit cell, the Green's function may be separated by splitting the limits of integration from $O(C)$ to $\frac{1}{2}\eta_2^1$ and from $\frac{1}{2}\eta_2^1$ to ∞.

Then $G^{(j,j')} = G^{(j,j')(1)} + G^{(j,j')(2)}$ where

$$G^{(j,j')(1)} = -\frac{1}{2\pi^{3/2}}\sum_s e^{i\vec{k}\cdot\vec{r}_s}\int_{O(c)}^{\frac{1}{2}\eta_2^1} e[-(\vec{R}_{jj'}+\vec{a}_j-\vec{a}_j-\vec{r}_s)^2\xi^2 + \kappa^2/4\xi^2]d\xi$$

and

$$G^{(j,j')(2)} = -\frac{1}{2\pi^{3/2}} \sum_s e^{i\vec{k}\cdot\vec{r}_s} \int_{\frac{1}{2}\eta^{\frac{1}{2}}}^{\infty} e[-(\vec{R}_{jj'}+\vec{a}_j-\vec{a}_{j'}-\vec{r}_s)^2\xi^2 + \kappa^2/4\xi^2]d\xi. \tag{65}$$

Another identity derived by Ewald (26) which is valid for ξ from $0(C)$ to $\frac{1}{2}\eta^{\frac{1}{2}}$ for $\eta > 0$ is

$$\sum_s \exp[-(\vec{R}_{jj'}+\vec{a}_j-\vec{a}_j-\vec{r}_s)\xi^2]e^{i\vec{k}\cdot\vec{r}_s} = \frac{e^{ik\cdot(\vec{R}_{jj'}+\vec{a}_j-\vec{a}_j)}\pi^{3/2}}{\tau\xi^3} \sum_n \exp[-(\vec{K}_n+\vec{k})^2/4\xi^2+i\vec{K}_n\cdot(\vec{R}_{jj'}+\vec{a}_j-\vec{a}_{j'})], \tag{66}$$

when this is substituted into $G^{(j,j')(1)}$ and the integration is performed then

$$G^{(j,j')(1)} = -\frac{1}{\tau} e^{E/\eta} \sum_n \frac{e^{i(\vec{K}_n+\vec{k})\cdot(\vec{R}_{jj'}+\vec{a}_j-\vec{a}_j)}e^{-(\vec{K}_n+\vec{k})^2/\eta}}{(\vec{K}_n+\vec{k})^2-E}. \tag{67}$$

If we use the plane wave expansion, Equation 29, on $G^{(j,j')(1)}$ and $G^{(j,j')(2)}$, equate the sum of these quantities to

$$G^{(j,j')} = \sum_{L,M} D_{LM}^{(j,j')} j_L(KR_{jj'})Y_{LM}(\hat{R}_{jj'}) - \frac{\delta_{jj'}}{4\pi}\frac{\cos KR}{R}, \tag{68}$$

multiply both sides by $Y_{LM}^{*}(\hat{R}_{jj'})$, integrate over spherical harmonics and taking the limit of $R_{jj'} \to 0$, we find that

$$D_{LM}^{(j,j')} = D_{LM}^{(j,j')(1)} + D_{LM}^{(j,j')(2)} + \delta_{jj'}\delta_{L0}\delta_{M0}D_{00}^{(3)}. \tag{69}$$

The values of the D coefficients are

$$D_{LM}^{(j,j')(1)} = -\frac{4\pi}{\tau} i^L \frac{e^{E/\eta}}{\sqrt{E^L}} \sum_n \times \frac{|\vec{K}_n+\vec{k}|^L e^{i(\vec{K}_n+\vec{k})\cdot(\vec{a}_j-\vec{a}_{j'})} e^{-(\vec{K}_n+\vec{k})^2/\eta} Y_{LM}^*(\hat{\vec{K}_n+\vec{k}})}{(\vec{K}_n+\vec{k})^2 - E}, \tag{70}$$

$$D_{LM}^{(j,j')(2)} = \frac{-2^{L+1}}{\sqrt{\pi}E^L} \sum_s{}' e^{i\vec{k}\cdot\vec{r}_s} |\vec{r}_s-\vec{a}_j+\vec{a}_{j'}|^L Y_{LM}^*(\vec{r}_s-\vec{a}_j+\vec{a}_{j'}) \times \int_{\frac{1}{2}\eta^{\frac{1}{2}}}^{\infty} d\xi\, \xi^{2\ell} \left[e^{-\xi^2(\vec{r}_s-\vec{a}_j+\vec{a}_{j'})^2 + E/4\xi^2}\right] \tag{71}$$

and

$$D_{00}^{(3)} = \frac{-\eta^{\frac{1}{2}}}{2\pi} \sum_{s=0}^{\infty} \frac{(E/\eta)^s}{s!(2s-1)}. \tag{72}$$

The sum in Equation 71 has the term s=0 omitted if j=j'.

In order to use the D coefficients in the secular determinant, it is necessary to find the relationship between the $A_{\ell m;\ell' m'}^{(j,j')}$ and $D_{LM}^{(j,j')}$ coefficients. Using the plane wave expansion Equation 29

$$e^{i\vec{K}\cdot\vec{R}_{jj'}} = 4\pi \sum_{\ell,m} i^\ell j_\ell(KR_{jj'}) Y_{\ell m}(\hat{R}_{jj'}) Y_{\ell m}^*(\theta_K,\phi_K)$$

multiplying both sides of this equation by $Y_{LM}(\theta_K,\phi_K)$ and integrating

over solid angle we get

$$j_L(\kappa R_{jj'})Y_{LM}(\hat{R}_{jj'}) = \frac{1}{4\pi i^L}\int e^{i\vec{\kappa}\cdot\vec{R}_{jj'}}Y_{LM}(\theta_\kappa,\phi_\kappa)\,d\Omega_\kappa.$$

$\vec{R}_{jj'}$ is defined as $\vec{R}_{jj'} = \vec{r}_j - \vec{r}'_{j'}$. If this is substituted into the previous equation and the plane wave expansion applied twice, then

$$j_\ell(\kappa R_{jj'})Y_{LM}(\hat{R}_{jj'}) = \frac{4\pi}{i^L}\sum_{\substack{\ell,m\\ \ell',m'}} i^{\ell-\ell'}j_\ell(\kappa r_j)j_{\ell'}(\kappa r'_{j'})Y_{\ell m}(\hat{r}_j)\times \qquad (73)$$

$$Y_{\ell'm'}(\hat{r}'_{j'})C^{LM}_{\ell m;\ell'm'}$$

where

$$C^{LM}_{\ell m;\ell'm'} = \int d\Omega_\kappa Y_{LM}(\theta_\kappa,\phi_\kappa)Y^*_{\ell m}(\theta_\kappa,\phi_\kappa)Y_{L'M'}(\theta_\kappa,\phi_\kappa). \qquad (74)$$

The coefficients C vanish unless $m = M+m'$, $|\ell-\ell'| \le L \le \ell+\ell'$ and $\ell+\ell'+L$ is an even integer. Equating Equations 68 and 59 and using Equations 70-72, we get the relation between the A and D coefficients,

$$A^{(j,j')}_{\ell m;\ell'm'} = 4\pi i^{\ell-\ell'}\sum_{L,M} i^L D^{(j,j')}_{LM} C^{LM}_{\ell m;\ell'm'}. \qquad (75)$$

The coefficients as defined in Equation 74 may be evaluated by using the composition relation for spherical harmonics

$$\int Y_{LM} Y_{\ell m} Y_{\ell' m'} d\Omega = \left(\frac{(2L+1)(2\ell+1)(2\ell'+1)}{4\pi} \right)^{\frac{1}{2}} \begin{pmatrix} L & \ell & \ell' \\ 0 & 0 & 0 \end{pmatrix} \begin{pmatrix} L & \ell & \ell' \\ M & m & m' \end{pmatrix} .$$

If we let $m \to -m$ then $Y_{\ell -m} = (-1)^m Y^*_{\ell m}$ and the C coefficients are given by

$$C^{LM}_{\ell m; \ell' m'} = (-1)^m \left(\frac{(2L+1)(2\ell+1)(2\ell'+1)}{4\pi} \right)^{\frac{1}{2}} \begin{pmatrix} L & \ell & \ell' \\ 0 & 0 & 0 \end{pmatrix} \begin{pmatrix} L & \ell & \ell' \\ M-m & m' \end{pmatrix} \qquad (76)$$

where $\begin{pmatrix} J_1 & J_2 & J_3 \\ m_1 & m_2 & m_3 \end{pmatrix}$ are the Wigner -3J symbols.

THE ENERGY BANDS OF RHENIUM TRIOXIDE

The energy eigenvalues of ReO_3 were calculated along the high symmetry directions of the Brillouin zone as shown in Figure 3. Eigenvalues were then calculated at a uniform mesh of 56 spaced points in the 1/48th zone and were then interpolated to give the energy levels at 10^6 points in the Brillouin zone. The mesh points for which the energy eigenvalues were calculated are shown in Figures 6 and 7. The interpolation was done by using spline fits (27) through the points at which eigenvalues had been calculated.

This process was done twice, once corresponding to the ReO_3 crystal with an equilibrium lattice constant and the second time with the lattice constant compressed by 2% corresponding to a hydrostatic pressure of 113kbar. The d bands, spin-orbit coupling not included as Mattheiss has done (10), are shown in Figures 8 and 9.

During the investigation of the density of states and the interpolated bands, it was observed that these bands were consistently lower than the calculated energies. The interpolated eigenvalues along the Γ to X direction are lower than the calculated bands by .001 rydberg. This causes the eigenvalues along other directions in the interpolated mesh to be lower than the calculated values at these points by as much as .004 or .005 rydberg in the $k_z = 0$ plane. This in turn causes a drop in the calculated value of the Fermi energy by many times more.

It was apparent that the Fermi energy would have to be determined by counting the number of states of the original mesh. There are 1000 mesh points in the Brillouin zone, so there will also be one thousand

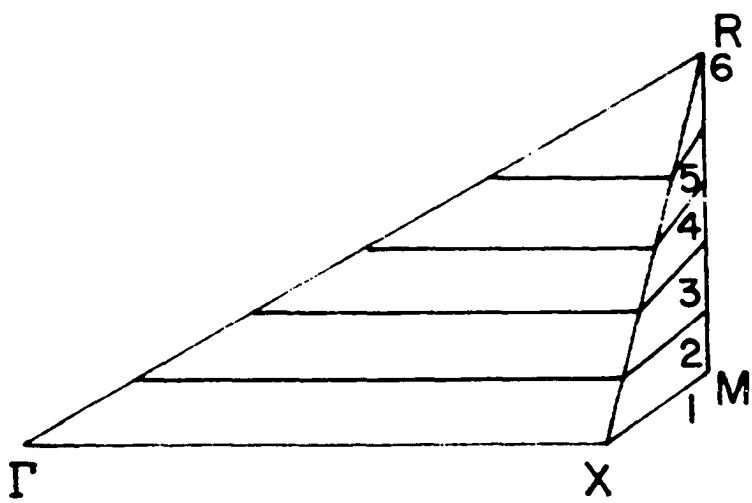

Figure 6. The 1/48th Brillouin zone showing the six layers in which energy eigenvalues were determined.

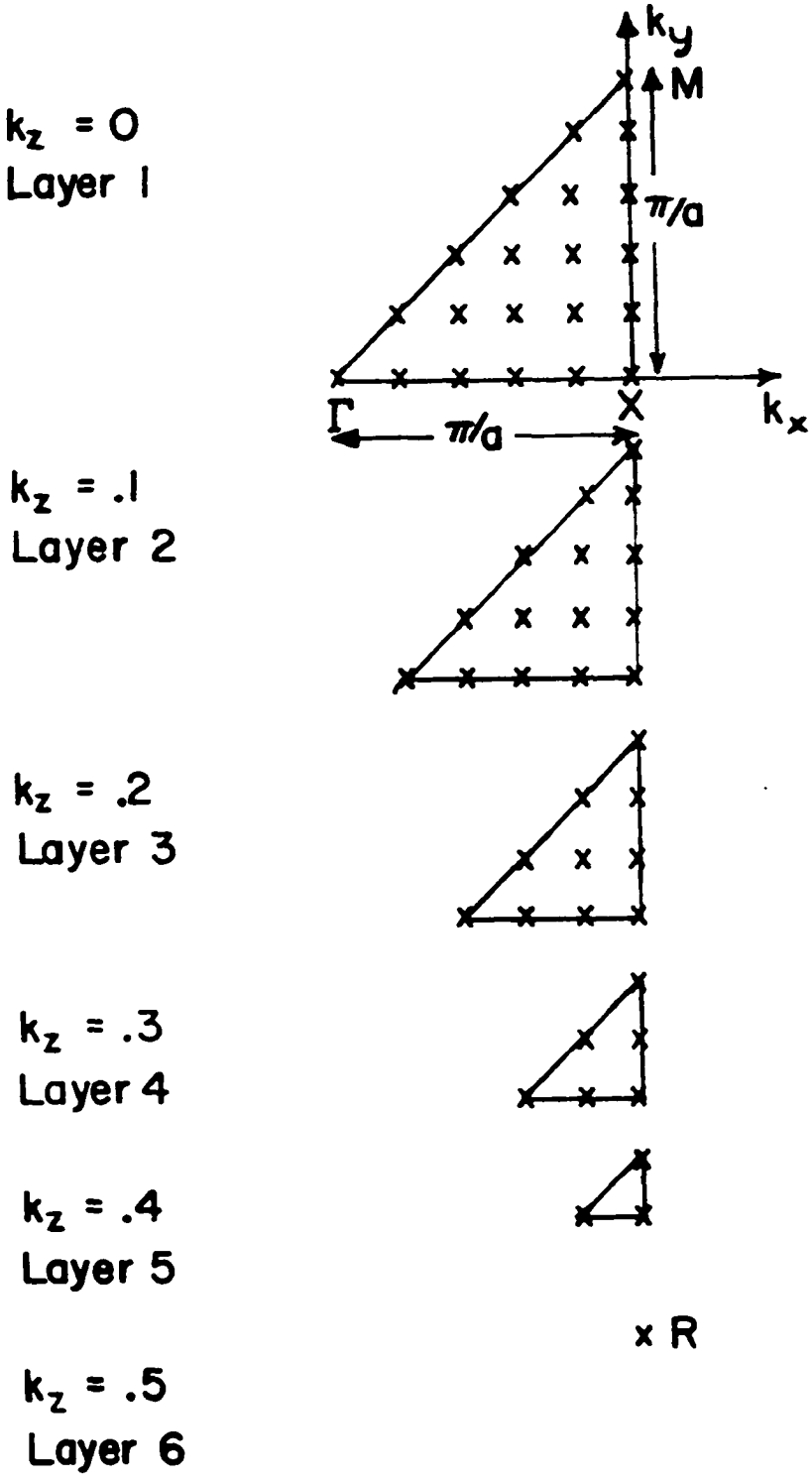

Figure 7. Cross sections of the 1/48th zone showing points at which energy eigenvalues were determined.

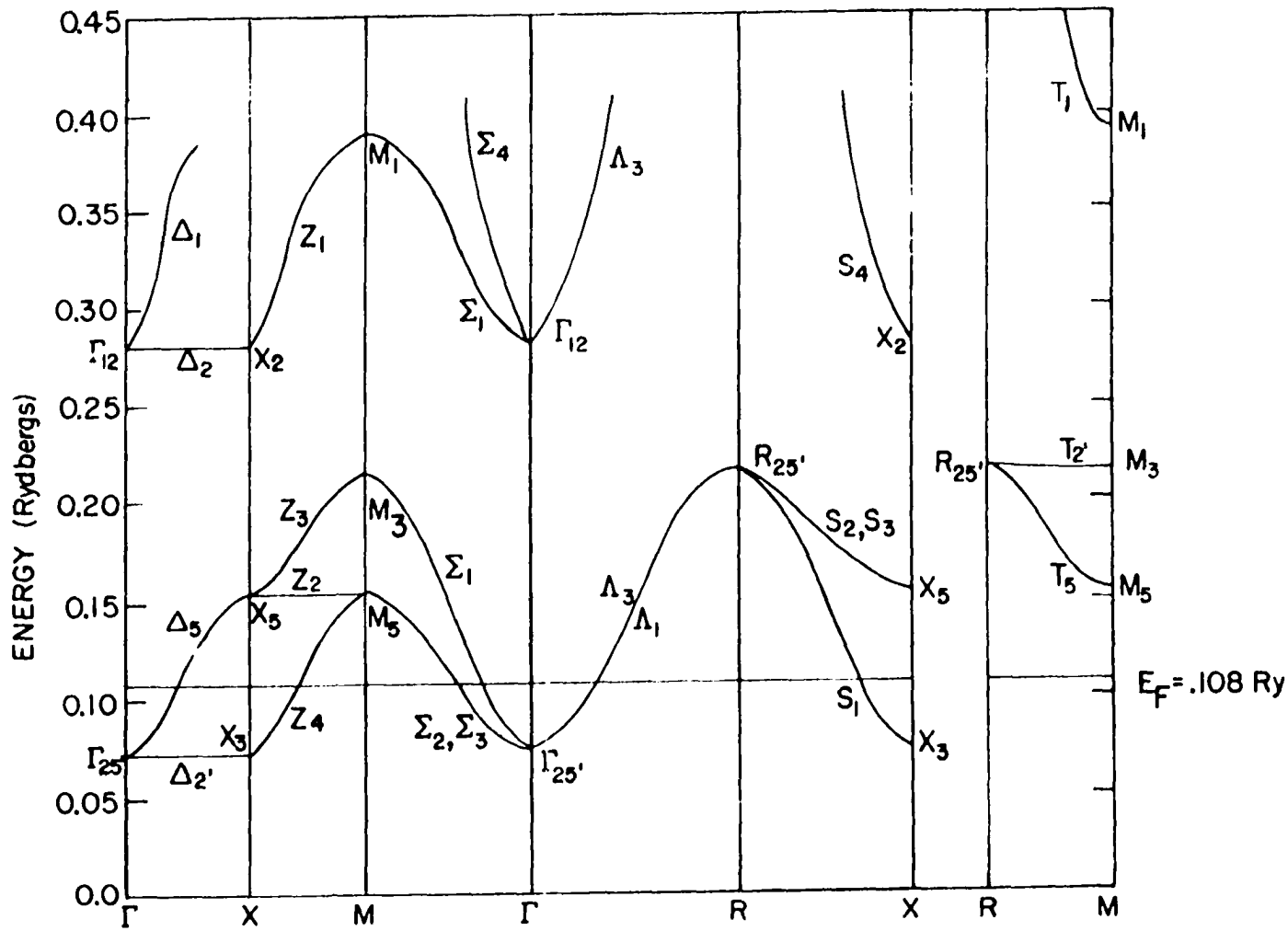

Figure 8. The electronic energy bands of ReO_3 for the equilibrium lattice constant.

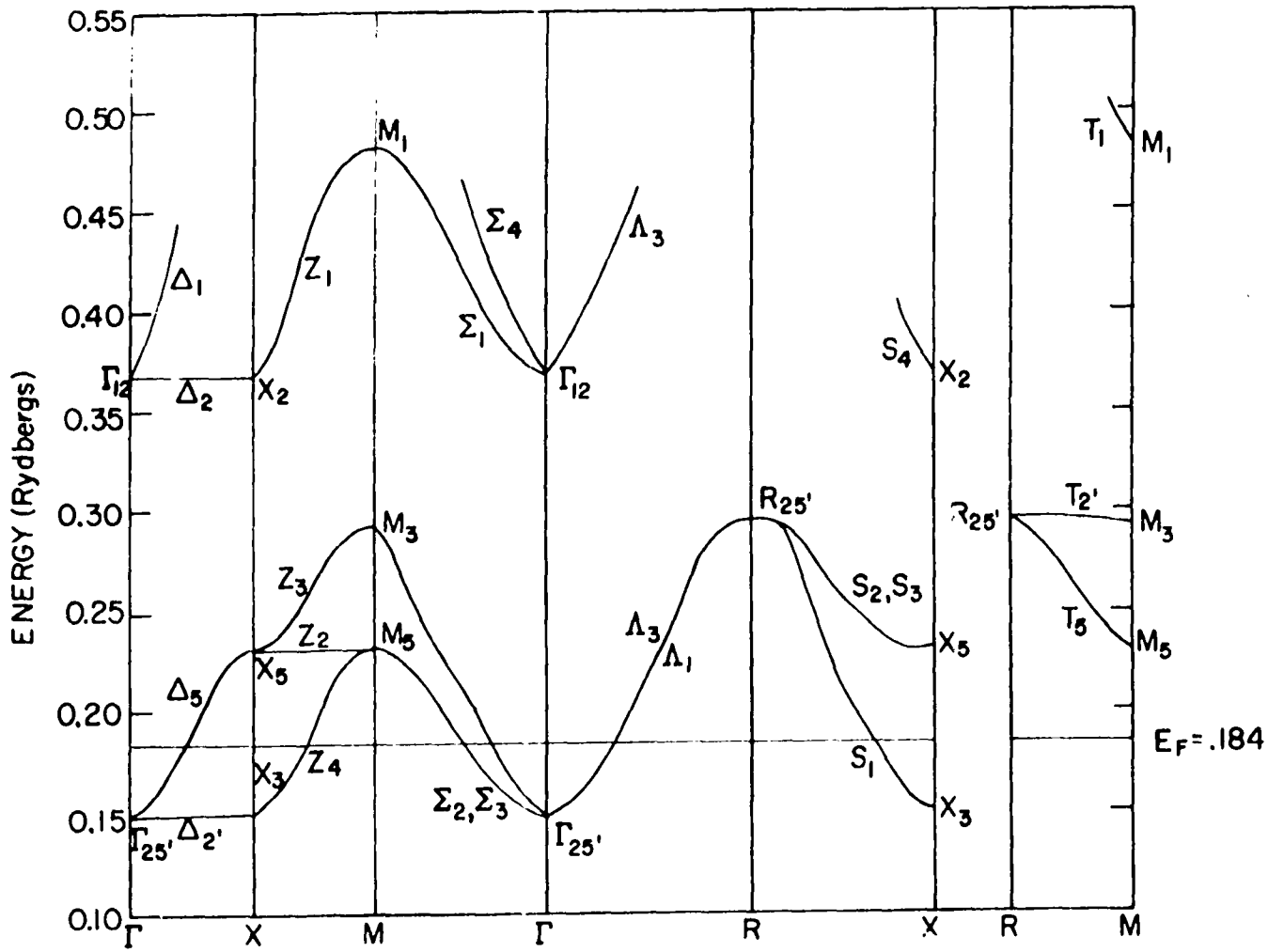

Figure 9. The electronic energy bands of ReO_3 for the equilibrium lattice constant compressed by 2%.

states which the one electron, which goes into the conduction band, will just fill at the Fermi energy. The Fermi energies were then determined to be at .108 Ry and .184 Ry instead of .097 Ry and .175 Ry, as determined from the interpolated bands, for the zero and high pressure bands respectively. The most probable reason for the failure of the Spline interpolation scheme is that the original mesh is not fine enough.

The density of states curves of ReO_3 for the equilibrium lattice constant and the lattice constant compressed by 2% are shown in Figures 10 and 11 respectively. The Fermi energy was found to lie at .108 Ry and .184 Ry which are .036 and .037 Ry above the bottom of the bands at the Γ point for the zero and high pressure cases respectively. The high pressure energy band of ReO_3 calculated by changing the lattice constant by 2% (see Table 3) has shifted the energy upward by .075 Ry at the Γ point and the width of the d band has increased slightly from $R_{25'}$ to $\Gamma_{25'}$.

The values of the density of states at the Fermi energy for the zero and high pressure cases are found to be 28.8 states/Ry-unit cell and 38.4 states /Ry-unit cell. Since we have considered 2 spin states per band the density of states at the Fermi energy, for each case, can also be quoted to be 14.4 states of one spin/Ry-unit cell and 19.2 states of one spin/Ry-unit cell.

Recently Keller (28) has measured the specific heat of ReO_3 at low temperatures. The electronic specific heat can be written as

$$C_e = \gamma T \tag{77}$$

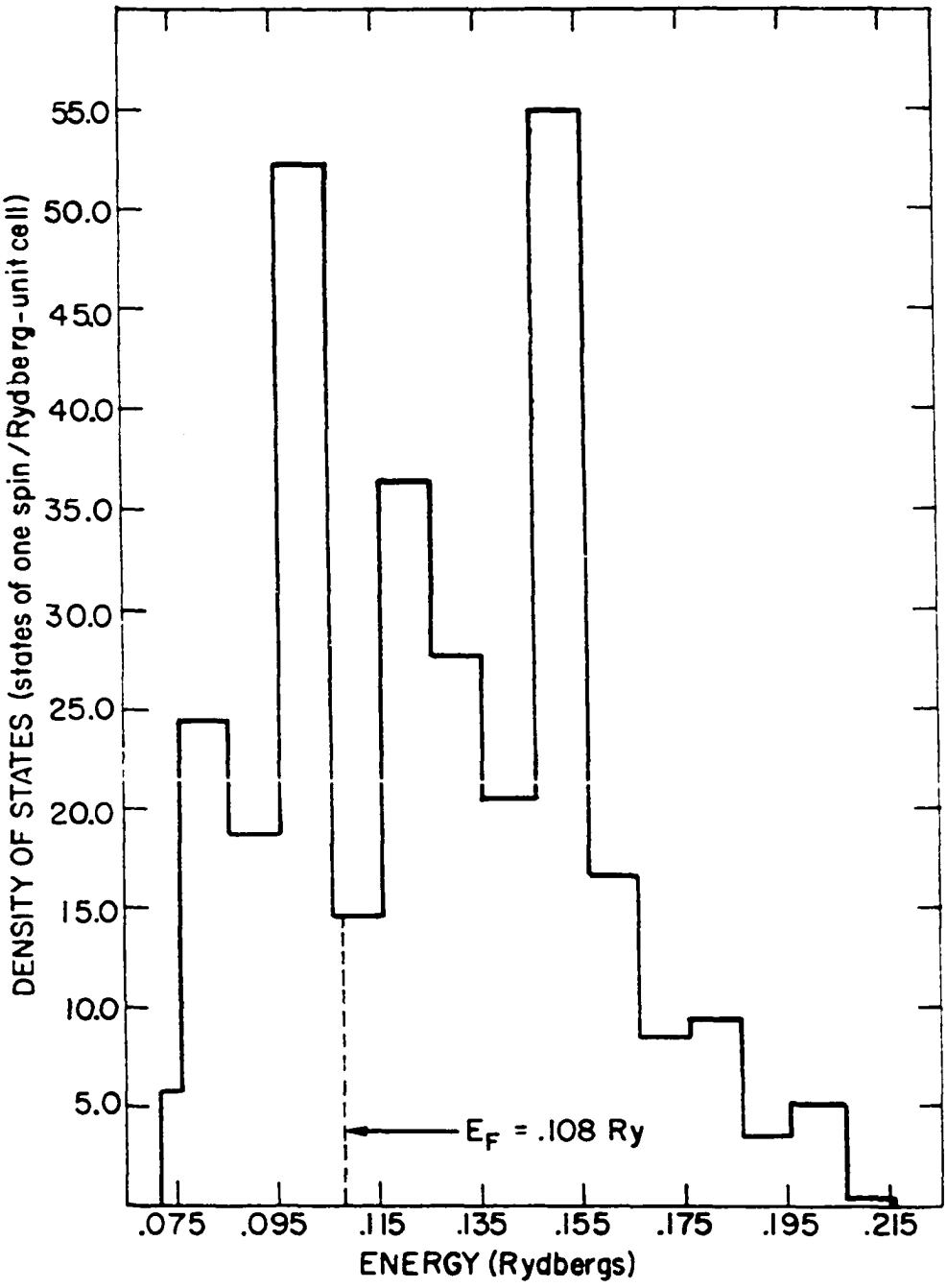

Figure 10. The density of states of ReO_3 for the equilibrium lattice constant.

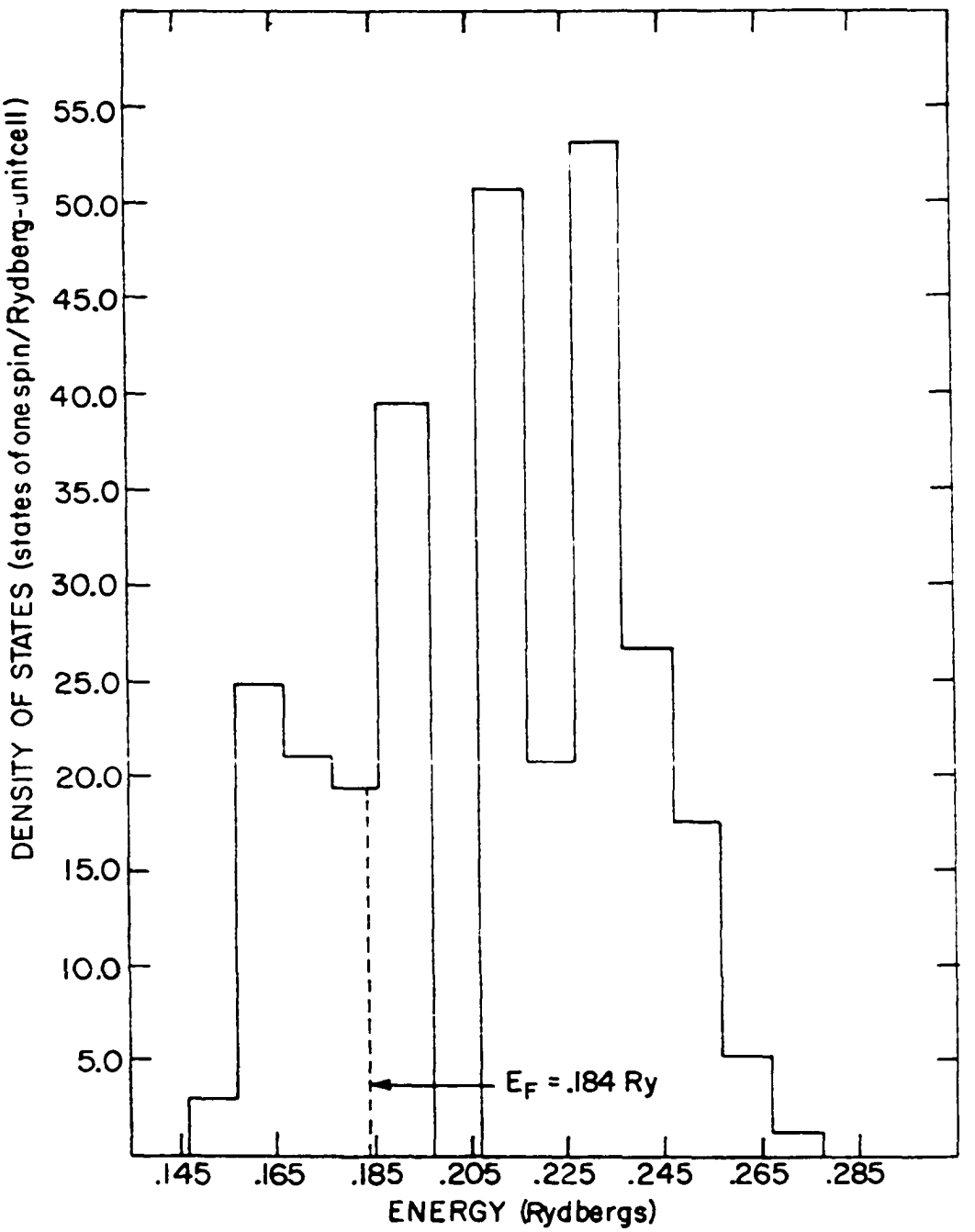

Figure 11. The density of states of ReO_3 for the equilibrium lattice constant compressed by 2%.

per mole where γ is related to the density of states at the Fermi energy by

$$\gamma = \frac{1}{3} \pi^2 k_B^2 V N(E_F), \tag{78}$$

where V is the molar volume, k_B is the Boltzman constant and $N(E_F)$ is the density of states at the Fermi energy. Keller obtained a value for γ of 2.85 mJ/mole-deg^2. Using the value of the density of states at the Fermi energy, for the equilibrium lattice constant, we obtain a value for γ of 2.68 mJ/mole-deg^2. This value is 6% smaller than the experimental value of Keller.

The small difference in the experimental and theoretical values for γ may be accounted for by mass enhancement of the electron via the electron phonon interaction which has not been included here. Since ReO_3 is a good metal whose conductivity is within an order of magnitude of copper at room temperature, we would not expect electrons and phonons to scatter appreciably and hence we obtain rather good agreement with the experimental value for γ. Using Mattheiss' (10,11) density of states at the Fermi energy, the value for γ is 2.50 mJ/mole-deg^2.

When the lattice constant is reduced by 2%, corresponding to a hydrostatic pressure of 113 kbar, the value of γ is 3.30 mJ/mole-deg^2. If we assume that the electron phonon interaction will again enhance the density of states by 6% at the Fermi energy, then the predicted value of γ is 3.51 mJ/mole-deg^2 at a pressure of 113 kbar. Since the number of states in the entire Brillouin zone is only 1000, $N(E_F)$ may be off by 50 to 100%.

THE FERMI SURFACE AND DE HAAS-VAN ALPHEN FREQUENCIES

The Fermi Surface

The Fermi surface of ReO_3 has three sheets corresponding to the three bands which cross the Fermi energy. Following the notation of Mattheiss, the three sheets are labeled α, β and γ. The α and β sheets are closed electron surfaces while the γ sheet is multiply connected. Figure 12 shows a slice of the three sheets of the Fermi surface along the [001] direction with the plane through the points Γ, X and M.

Three dimensional sketches of the α, β and γ sheets of the ReO_3 Fermi surface are illustrated by Mattheiss (10) and Phillips and Shanks (29) and are shown in Figures 13a, b and c. In the (100) planes the α sheet is almost circular while the β sheet is square with rounded edges in the [110] direction. This is shown in Figure 14. The γ sheet gives rise to a multiply connected piece of Fermi surface whose features are best described as 3 mutually orthogonal intersecting cylinders centered about the Γ point. As seen from Figure 12, all the sheets of the Fermi surface are centered aroud the Γ point.

The Pressure Derivatives of de Haas-van Alphen Frequencies

The sheets of the Fermi surface calculated by decreasing the lattice constant by 2% have the same general features as the original sheets of the Fermi surface. Free-electron scaling (15) predicts that the same fraction of the Brillouin zone remain filled by the electrons as a function of pressure.

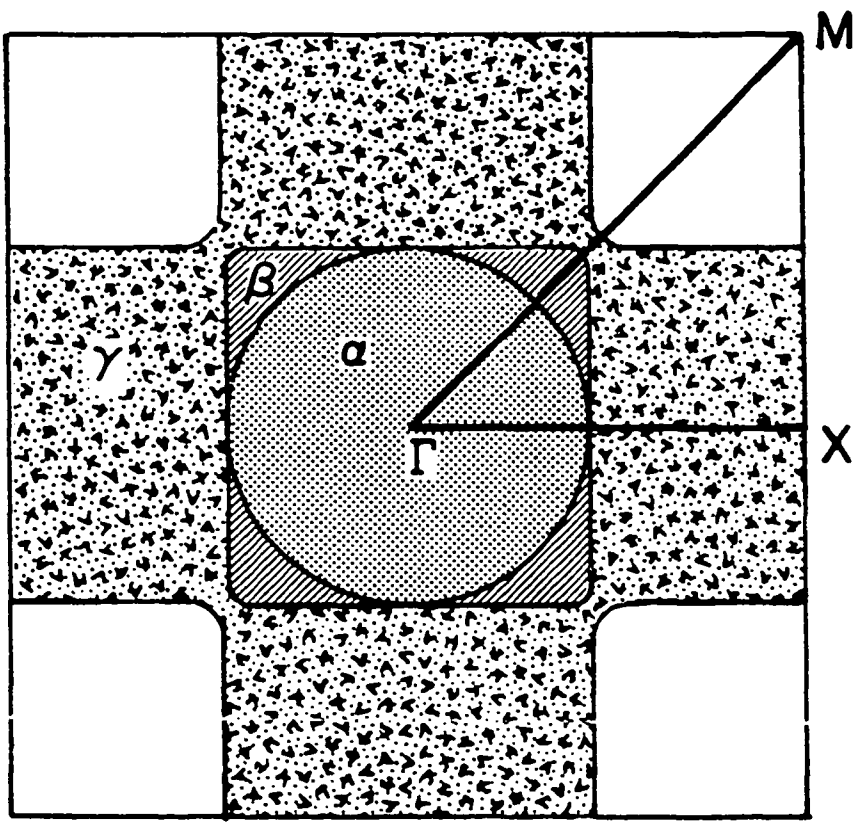

Figure 12. The cross sections of the 3 sheets of the Fermi surface in the [001] direction through the plane determined by the points Γ, X and M.

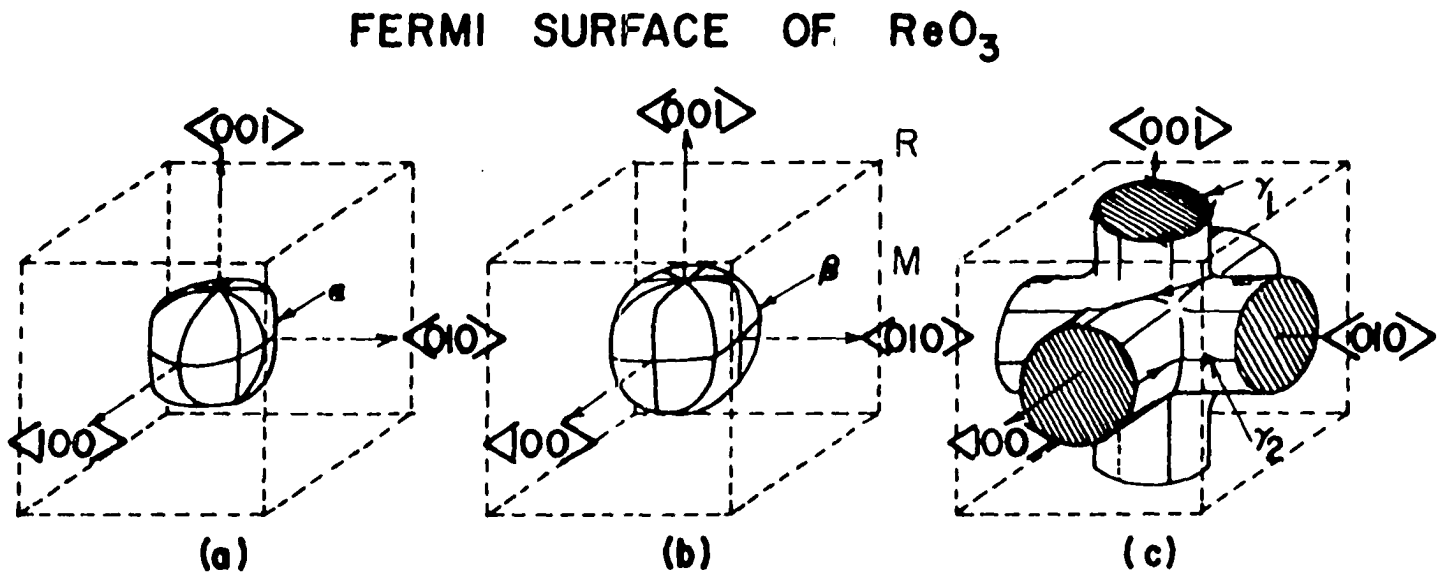

Figure 13. Three-dimensional sketches of the three electron sheets of the Fermi surface in ReO_3 (after Mattheiss (10)).

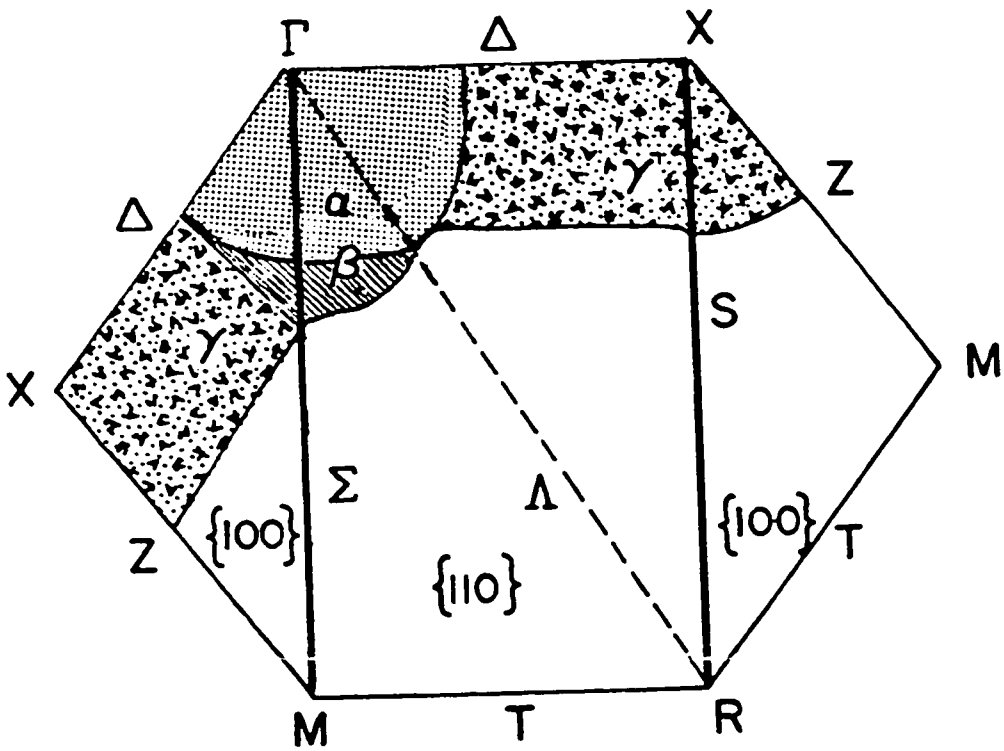

Figure 14. Central [110] and [100] cross sections of the ReO_3 Fermi surface.

Scaling then requires that the logarithmic derivative of the de Haas-van Alphen (dHvA) frequencies with respect to pressure

$$\frac{d\ell nF}{dp} = -\frac{K}{3}\,\ell n(F_2/F_1)/\ell n(a_2/a_1) \tag{79}$$

increase at a rate of two-thirds the volume compressibility for all cross sections of the Fermi surface.

This can easily be shown by the following arguments. Since the frequency in MG is related to the extremal areas by

$$F = 374.1 \times A_{(\text{extremal})}, \tag{80}$$

then

$$F_2/F_1 = \frac{A_{(\text{extremal})1}}{A_{(\text{extremal})2}}. \tag{81}$$

Since the scaling model predicts that the same fraction of the Brillouin zone remain filled then it follows that

$$\frac{A_{(\text{extremal})1}}{A_{\text{zone 1}}} = \frac{A_{(\text{extremal})2}}{A_{\text{zone 2}}} \tag{82}$$

or

$$\frac{A_{(\text{extremal})1}}{A_{(\text{extremal})2}} = \frac{a_1^2}{a_2^2}. \tag{83}$$

Substituting back into equations 79 and 81, we get

$$\frac{d\ell nF}{dp} = 2/3\ \kappa$$

or when $\kappa = 5.3 \times 10^{-4}$ kbar^{-1}

$$\frac{d\ell nF}{dp} = 3.6 \times 10^{-4} \text{ kbar}^{-1}. \tag{84}$$

This is the scaling prediction.

Experimental work by Schirber et al. (15) on ReO_3 shows that free-electron scaling fails to predict the rate at which all sheets of the Fermi surface change with respect to pressure. The experimental values and our results of the pressure derivatives of the Fermi surface cross sections are given in Table 4.

Even though the very simple free-electron scaling model predicts the same pressure derivatives for all the Fermi surface cross sections, it does give excellent agreement with the experiment and the results of this work for the α sheet in both the [001] and [111] field directions. The pressure derivative calculated in this work of the γ_2 orbit, the hole orbit, in the [001] field direction also agrees quite well with the scaling prediction.

The failure of the scaling prediction occurs in both the γ_1 and β orbits in the [001] field direction. There have been attempted measurements of the pressure derivatives of the β orbits but the amplitudes have not been sufficient to obtain a pressure derivative (15).

Table 4. Theoretical and experimental values for pressure derivatives of cross sectional areas of the Fermi surface of ReO_3

Cross section	Field direction	$d\ell nF/dp$ (10^{-4} $kbar^{-1}$) Experiment (15)	Theory
α	[001]	4.0 ± .3	3.74
	[111]	4.0 ± .4	3.64
β	[001]	none	6.42
γ_1	[001]	1.5 ± .5	0.64
γ_2	[001]	none	3.76

Scaling prediction $\sim 3.6 \times 10^{-4}$ $kbar^{-1}$

The de Haas-van Alphen Frequencies

The angular dependence of the de Haas-van Alphen (dHvA) frequencies have been measured by Marcus (13), Graebner and Greiner (30) and Phillips and Shanks (29). The calculated and experimental values of the dHvA frequencies in ReO_3 for high symmetry directions are shown in Table 5.

The calculated values of the frequencies agree reasonably well with the experimental values. The largest discrepancy ($\sim$ 10%) occurs in α branch in the [001] direction. The β branch has the smallest discrepancy with an error of approximately 1.5% in the [001] direction.

The α, β and γ_1 branches all give rise to electron orbits as shown in Figures 13a, b, and c. The γ_2 orbit is a hole orbit and its frequency has only been calculated here in the [001] direction. Marcus (13) and Graebner and Greiner (30) have not reported this orbit, but the agreement with our calculation and the work of Phillips and Shanks is within 6%. The γ_3 and γ_4 orbits have not been investigated here.

We have calculated the angular dependence of the dHvA frequencies from zero to 80 MG for field directions lying in the (010) and $(1\bar{1}0)$ planes. These results have been plotted on the same graph as the experimental results of Phillips and Shanks (29) and are shown in Figure 15. The dotted lines are the experimental results and the solid lines are the calculated results of this work.

The calculated α frequencies lie above the corresponding experimental points by approximately 5 MG. The shape of the experimental and calculated curves are very close except near the [111] direction in the $(1\bar{1}0)$ plane. The α branch of the Fermi surface as shown in Figures

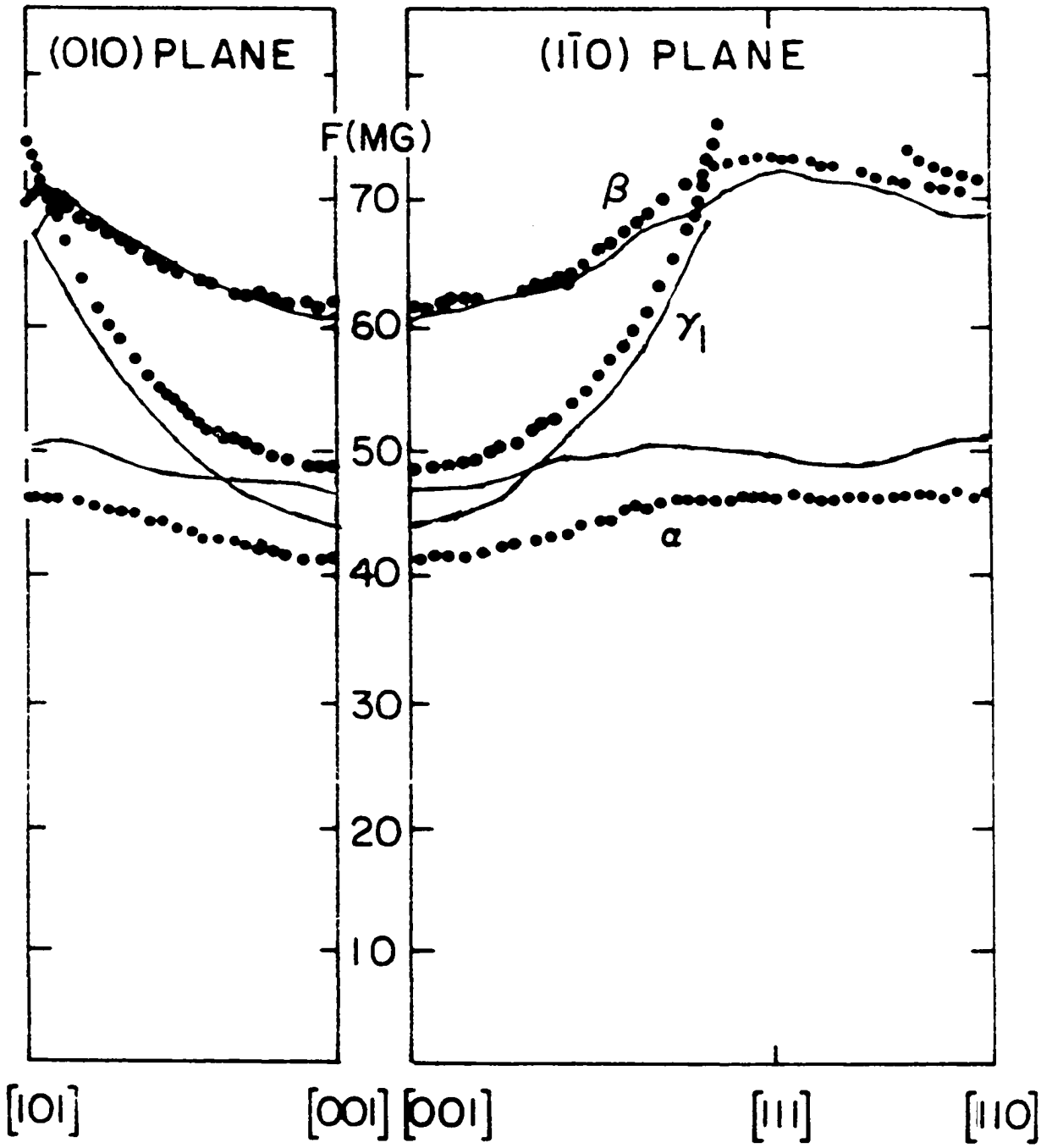

Figure 15. Variations of the de Haas-van Alphen frequencies between 40 and 80 MG. The solid lines are the calculated values and the dotted lines are the experimental results of Phillips and Shanks (29).

Table 5. de Haas-van Alphen frequencies in ReO_3 for high symmetry directions

Orientation	Branch	Calculated	Frequency in MG		
			Phillips and Shanks (29)	Marcus (13)	Graebner and Greiner (30)
[001]	α	46.8	41.5	41.4	42.0
	γ_1	43.7	48.8	48.8	49.5
	β	60.5	61.6	61.8	60.0
	γ_2	92.9	87.8	--	--
[111]	α	49.8	46.3	46.1	--
	β	72.7	73.2	73.4	75.0
[110]	α	51.0	46.3	46.2	47.5
	β	68.5	70.3	73.5	--
	γ_1	--	71.1	71.1	--

12-14 are nearly spherical and therefore we obtain dHvA frequencies which do not vary a great deal as a function of field direction.

Comparison of the β branch of the Fermi surface with the experimental results is quite good. The largest variation of our theoretical curve from the experimental work is $\sim 4\%$. However, the comparison of the angular dependence of β branch in the (010) and $(1\bar{1}0)$ planes is usually 1%. The orbits of this branch for different field directions are multiple valued functions and their extremal orbits were extremely difficult to calculate.

The γ_1 frequency branch is also an electron surface which arises from the arms of the γ branch of the Fermi surface. The largest error between the experimental and calculated values of this orbit occurs in the [001] field direction (~ 5 MG). As we move away from the [001] direction in both the (010) and $(1\bar{1}0)$ plane the discrepancy decreases. This frequency branch extends to the [111] direction in the $(1\bar{1}0)$ plane. Marcus (13) and Phillips and Shanks (29) report that the γ_1 branch is also centered around the [110] direction in the $(1\bar{1}0)$ plane. We were unable to locate the γ_1 branch in this direction.

SUMMARY AND CONCLUSIONS

This investigation has dealt with the electronic band structure of the transition metal oxide ReO_3 and the relationship of the band structure to the electronic properties of this crystal for its equilibrium lattice constant and a compressed lattice constant. We have employed the KKR method to calculate the band structure of this compound. Throughout this investigation there have been no adjustable parameters or fits to any experimental data. Thus this has been an attempt at a genuine "first principles" calculation of the electronic structure of ReO_3.

The energy eigenvalues of the ReO_3 crystal were calculated twice at a uniform mesh of 56 points in the 1/48th zone, once corresponding to the crystal with the equilibrium lattice constant and the second time with the lattice constant compressed by 2% corresponding to a hydrostatic pressure of 113 kbar. The Fermi energy was found to lie at .108 Ry and .184 Ry which are .036 and .037 Ry above the bottom of the bands at the Γ point for the equilibrium and compressed cases respectively. The shape of the energy bands for both cases are very similar. The energies of the compressed crystal are shifted upward by .075 Ry at the Γ point and the width of the d band has decreased by approximately .01 Ry at M.

Using the density of states at the Fermi energy, for the equilibrium lattice constant, we obtain a value for γ, the electronic contribution to the specific heat, to be 2.68 mJ/mole-deg^2. This is 6% smaller than the experimental value of Keller (28). The small difference

in the experimental and calculated values for γ may be accounted for by the mass enhancement of the electrons via the electron phonon interaction which we have not included here. The gap seen in the density of states for the non equilibrium lattice constant, Figure 11, is not a true gap in the density of states. This gap arises because the number of states used to determine this curve was only 1000. The interpolation scheme failed since the original mesh was not fine enough. The gap occurs since there were no eigenvalues present in this energy range.

The Fermi surface of ReO_3 has three sheets corresponding to the three bands which cross the Fermi energy, Figures 12-14. The α sheet is a closed electron surface centered around Γ and is a nearly spherical electron surface. The β sheet is also a closed electron surface centered around Γ. It is has a square-like shape with rounded edges in the [110] direction of the (001) plane. The γ sheet is a multiply connected piece of Fermi surface. Its features are best described as three mutually orthogonal intersecting cylinders centered about the Γ point.

The calculated values of the de Haas-van Alphen frequencies agree reasonably well with the experimental values (13) and (29-30). The largest discrepancy occurs in the α branch in the [001] direction ($\sim$ 10%). The β branch has the smallest error of 1.5% in the [001] direction. γ_2 is a hole orbit whose value has been calculated here only in the [001] direction. Its agreement with the work of Phillips and Shanks is within 6%. The γ_1 frequency branch which arises from the arms of the γ branch of the Fermi surface has a maximum deviation from

experiment of 5MG in the [001] field direction. As we move away from the [001] direction in both the (010) and $(1\bar{1}0)$ plane, the discrepancy decreases.

Free-electron scaling predicts that the fraction of the Brillouin zone which remains filled by the electrons is independent of pressure. This requires that the logarithmic derivative of the de Hass-van Alphen frequencies with respect to pressure be equal to two thirds times the bulk compressibility. Even though the free-electron scaling model predicts the same pressure derivatives for all branches of the Fermi surface it does give excellent agreement with the experimental work by Schirber et al. (15) and the results of this calculation for the α sheet in the [001] and [111] field directions and the γ_2 hole orbit in the [001] field direction. The failure of the scaling prediction occurs for both the γ_1 and β orbits according to the results of this work. Pressure data available from experimental work (15) for the γ_1 orbit also shows marked deviation from the free-electron scaling model.

BIBLIOGRAPHY

1. A. Ferretti, D. B. Rogers, and J. B. Goodenough, J. Phys. Chem. Solids 26, 2007 (1965).

2. J. Feinleib, W. J. Scouler, and A. Ferretti, Phys. Rev. 165, 765 (1968).

3. A. T. Fromhold, Jr., and Albert Narath, Phys. Rev. 152, 585 (1966).

4. M. J. Sienko, Advances in Chemistry edited by R. Ward (American Chemical Society, Washington D.C. 1963) Series 39.

5. J. M. Keller, J. Chem. Phys. 33, 232 (1960).

6. A. R. Mackintosh, J. Chem. Phys. 38, 1991 (1963).

7. R. Fuchs, J. Chem. Phys. 47, 3781 (1965).

8. J. B. Goodenough, P. Gibart, and J. Brenet, Compt. Rend. 261, 2331 (1965).

9. Albert Narath and D. C. Barham, Phys. Rev. 176, 479 (1968).

10. L. F. Mattheiss, Phys. Rev. 181, 987 (1969).

11. L. F. Mattheiss, Phys. Rev. B 2, 3918 (1970).

12. J. C. Slater and G. F. Koster, Phys. Rev. 94, 1498 (1954).

13. S. M. Marcus, Phys. Letters 27A, 584 (1968).

14. W. B. Pearson, A Handbook of Lattice Spacings and Structures of Metals and Alloys (Pergamon, New York, 1958).

15. J. E. Schirber, B. Morosin, J. R. Anderson, and D. R. Stone, Phys. Rev. B 5, 752 (1972).

16. B. Segall, Phys. Rev. 105, 108 (1957).

17. J. Korringa, Physica 13, 392 (1947).

18. W. Kohn and N. Rostoker, Phys. Rev. 94, 1111 (1954).

19. F. S. Ham and B. Segall, Phys. Rev. 124, 1786 (1961).

20. L. F. Mattheiss, Phys. Rev. 133, A1399 (1964).

21. F. Herman and S. Skillman, Atomic Structure Calculations (Prentice Hall, Inc., Englewood Cliffs, N. J., 1963).

22. J. C. Slater, Phys. Rev. 81, 385 (1951).

23 P. O. Löwdin, Advan. Phys. 5, 1 (1956).

24. J. M. Ziman, Electrons and Phonons (Oxford University Press, Amen House, London, 1961).

25. J. D. Jackson, Classical Electrodynamics (Wiley, New York, 1962).

26. P. Ewald, Ann. Phys. 64, 253 (1921).

27. Ralph H. Pennington, Introductory Computer Methods and Numerical Analysis (Macmillan, New York, 1965).

28. D. Keller, Ph.D. thesis, Iowa State University, 1970 (unpublished).

29. R. A. Phillips and H. R. Shanks, Phys. Rev. B, 4, 4601 (1971).

30. J. E. Graebner and E. S. Greiner, Phys. Rev. 185, 992 (1969).

ACKNOWLEDGMENTS

The author is deeply indebted to many people for the successful completion of this work. Professor S. H. Liu is thanked for his unending confidence and help during the author's first several years of graduate school, for the suggestion of this problem, and for his continued interest and help during this investigation. Deep thanks are given to Professor S. K. Sinha for his help and friendship during the last months of this investigation. Very special gratitude and thanks are given to Dr. R. P. Gupta for all the time he spent in discussing the many computer programs required to complete this investigation.

The author also thanks his wife, Jan, for her patience during the duration of this work. Her continued confidence helped especially during the frustrating period of time. Also, he would like to thank Jan for typing this manuscript.

Thanks are given to the Computer Center staff for their assistance and to the Ames Laboratory for their financial support during the course of study.

Finally, the author thanks his brother and parents for encouraging his study.